EQCM · 6-HOUR SHORT COURSE

MODULE 3

Applications of EQCM

Apply EQCM to five major application areas — electrodeposition, corrosion, batteries, supercapacitors, polymers, sensors and bioelectrochemistry — and recognize the specific advantages, limitations, and best practices in each case.

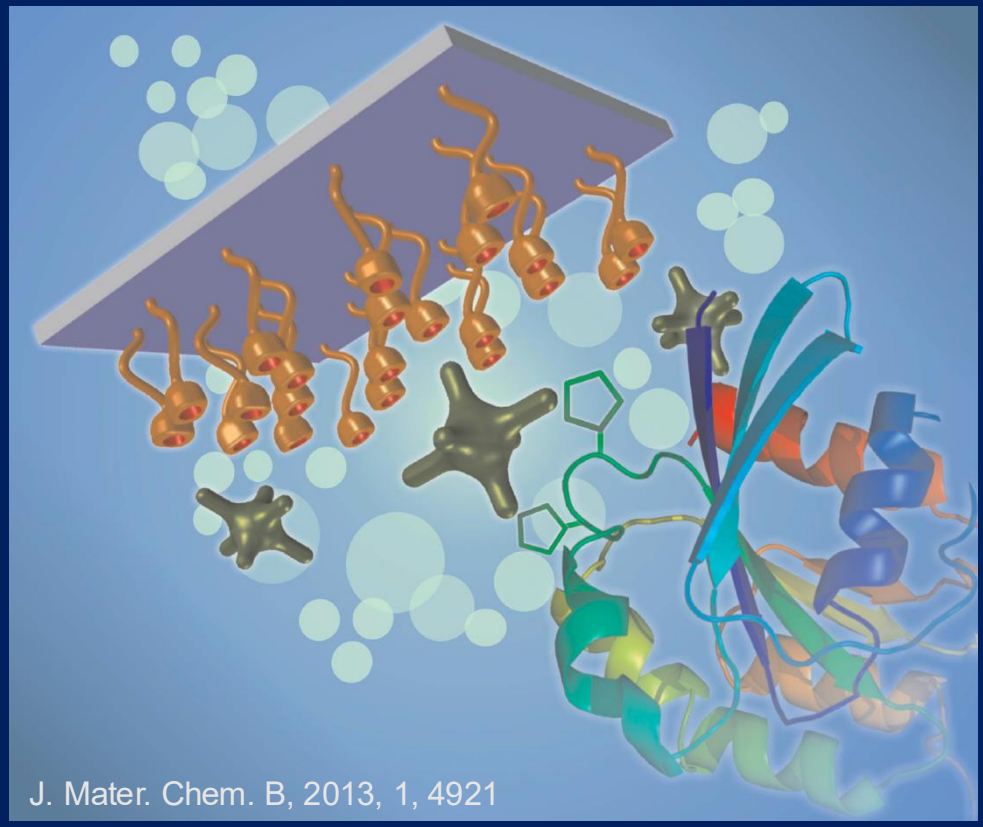

J. Mater. Chem. B, 2013, 1, 4921

Roberto M. Torresi

Depto. Química Fundamental, Instituto de Química, Universidade de São Paulo, São Paulo, Brasil

e-mail: rtorresi@iq.usp.br

The Electrochemical Quartz Crystal Microbalance in Electrodeposition

Real-time gravimetry of metal deposition — **kinetics · efficiency · nucleation · alloys & additives**

$\Delta f \propto \Delta m$
Sauerbrey gravimetry

Massograms
$d\Delta m/dt$ vs E

Speciation
bulk → interface

Based on five case studies: Mn·NH_4SCN (Electrochim. Acta 2006) · In nucleation (Electrochim. Acta 2023) · MnO_2 review (ChemSusChem 2025) · Mg mixed-anion EQCM-D (J. Mater. Chem. A 2026) · Pt MOR (Inorganics 2025)

FOUNDATION

Why EQCM for electrodeposition?

The Sauerbrey principle

$$\Delta f = -Cf \cdot \Delta m$$

A rigidly-coupled mass change on the resonator shifts its frequency in direct, nanogram-scale proportion. A 5 MHz crystal resolves ~ng·cm^{-2} changes in situ, in real time.

ng·cm^{-2}
mass resolution

real-time
in-situ signal

dΔm/dt
→ massograms

When ΔD ≈ 0 the layer is rigid and Sauerbrey holds; a rising dissipation (ΔD) flags a soft / viscoelastic / porous film — a caution, and also information.

Deposition kinetics
Mass flux vs. potential/time, decoupled from bulk current.

Current efficiency
Gravimetric Δm vs. Faraday's-law charge → % efficiency & M/z.

Nucleation & growth
Detects deviations from ideal 2D / 3D diffusion-controlled models.

Alloys & additives
Tracks co-deposition, surfactant/ion incorporation, dissolution.

Framing: Zong 2025 (Eq. Sauerbrey) · Yang 2026 (ΔD, EQCM-D)

3.1 · POINT 1

Real-time monitoring of deposition kinetics

Massograms: dΔm/dt vs. E

Plotting the **rate of mass change** against potential gives a curve analogous to a voltammogram — but **immune to the hydrogen-evolution current** that swamps the CV.

Sign convention

- negative flux → reduction (mass gain)
- positive flux → oxidation / dissolution (mass loss)
- positive flux with no anodic current → non-faradaic dissolution

The cross-over potential (E_{co}) read from the massogram tracks the reversible Mn(II)/Mn(0) potential — unreachable from the CV alone.

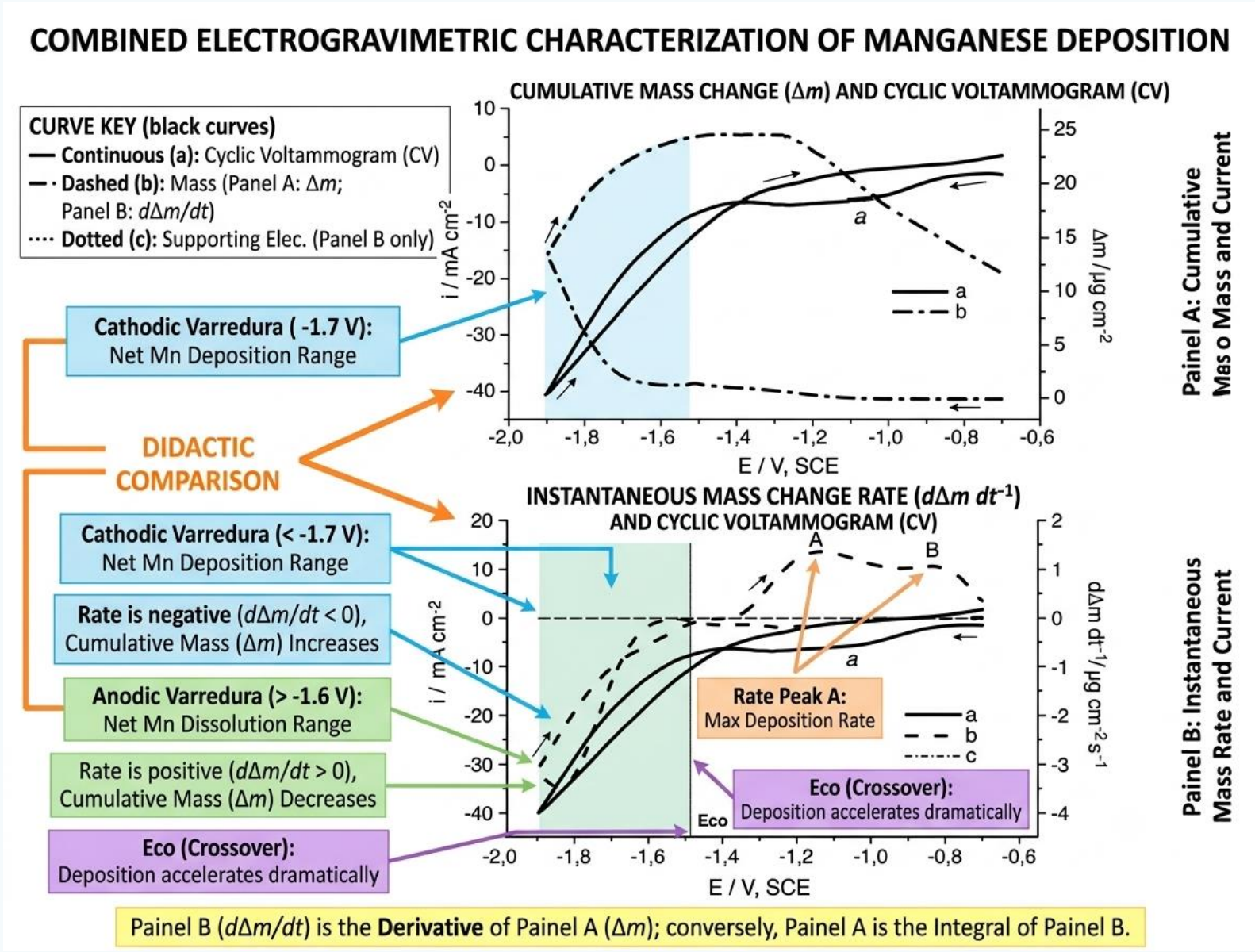

FIGURES: Fig. 2 & Fig. 3 — Díaz-Arista et al., Electrochim. Acta 51 (2006) 4393

3.1 · POINT 2

Current efficiency: Faraday's law vs. gravimetric mass

The M/z read-out

$$M/z = (\Delta m / \Delta Q) \cdot F$$

Combining the EQCM mass change with the charge passed yields the experimental mass-per-electron. Compared to the theoretical value for a reaction, it reveals:

- parasitic charge (HER) → experimental M/z below theoretical
- low-valent / soluble intermediates → M/z above theoretical
- passivation / film formation → depressed M/z

Since HER consumes charge but adds no mass, the gap is a direct, in-situ efficiency gauge.

Indium on Pt — current efficiency falls as potential rises

Electrodeposition current isolated from total current via the EQCM mass signal; HER intensifies at more negative potential.

Potential (V)	Deposit mass (ng)	Charge (C)	Efficiency (%)
−0.81	39096	0.116	84.96
−0.82	40211	0.126	80.64
−0.84	38613	0.125	77.69
−0.86	35478	0.117	76.57
−0.90	32691	0.109	75.63

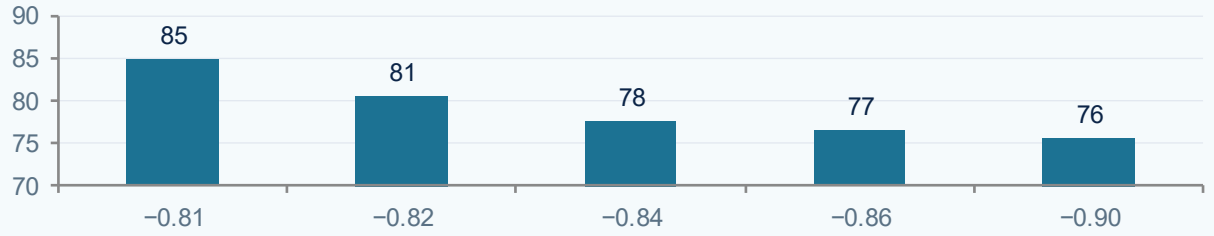

FIGURE/DATA: Table 2 & Eq. (1)–(2) — Hu et al., Electrochim. Acta 443 (2023) 141963

3.1 · POINT 3

Nucleation & growth: deviations from ideal models

Scharifker–Hills, cleaned up

Current transients are fit to **instantaneous** vs. **progressive** 3D nucleation. But when HER runs alongside deposition, the transient is distorted and the fit misleads.

EQCM fix

- mass is blind to HER → differentiate Q(t) from Δm(t) to recover the true deposition current transient
- reconstructed j(t) reproduces nucleation rise + diffusion-zone overlap decay

Indium: GC follows progressive nucleation; on Pt the regime shifts from instantaneous → progressive as adsorbed H is displaced. D ≈ 1.2–1.3 × 10^{-5} $cm^2 \cdot s^{-1}$.

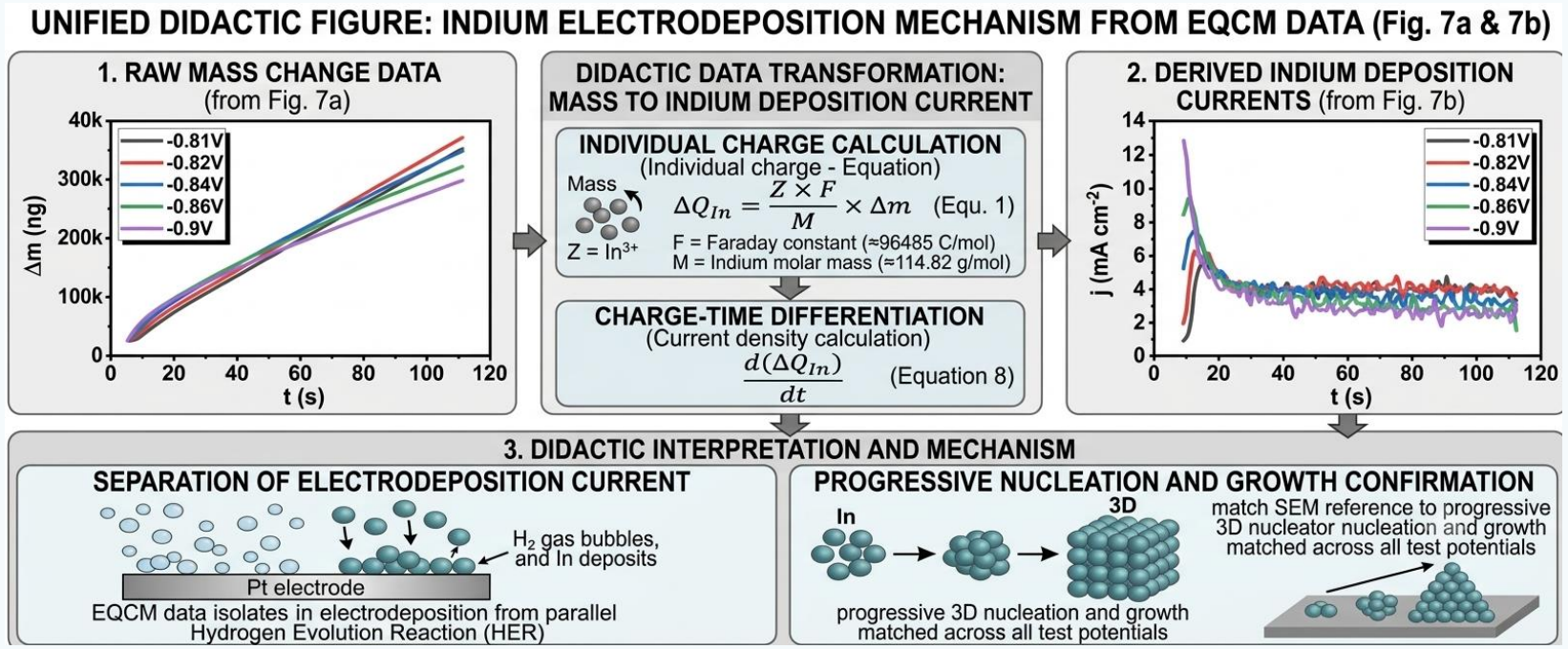

FIGURES: Fig. 5, Fig. 8 & Eq. (3)–(11) — Hu et al., Electrochim. Acta 443 (2023) 141963

3.1 · POINT 4

Co-deposition of alloys & incorporation of additives

Alloy / phase co-deposition

With NH_4SCN, EQCM massograms resolve two distinct dissolution peaks (I_a', H') — the fingerprints of separate α- and γ-Mn phases co-deposited from one bath.

α + γ manganese

Díaz-Arista 2006 · Fig. 8–12

Additive incorporation

Thiocyanate shifts the cross-over potential (complexation with Mn^{2+}) and suppresses $Mn(OH)_2$ adsorption — the mass signal quantifies what the additive changes at the surface.

SCN^- complexation

Díaz-Arista 2006 · Fig. 6

Surfactants & templates

EQCM tracks MnO_2 deposition rate under SDS / CTAB and cationic-surfactant intercalation, distinguishing layered δ-MnO_2 growth from compact films.

SDS / CTAB / C_n^+

Nakayama 2025 · §3.1.3, Fig. 3–4

The gravimetric channel separates faradaic co-deposition from non-faradaic adsorption/inclusion — invisible to the CV alone.

Massograms distinguish which mass is metal, which is hydroxide, and which is trapped additive.

3.1 · CASE STUDY

Metal electrodeposition followed by EQCM(-D)

Beyond mass: EQCM-D adds dissipation (ΔD) across overtones, turning the balance into an in-situ probe of **viscoelasticity, porosity and solvent coupling** of the growing deposit.

Workflow — Mg plating in mixed-anion electrolytes

1. **OCP loading**
   Gordon–Kanazawa ρη from Δf → interfacial viscosity
2. **Pre-deposition**
   Δm–ΔQ slope (mpe) reveals adsorbed CIPs / solvated complexes
3. **Nucleation & growth**
   Sauerbrey → hydrodynamic model as film turns porous
4. **Stripping**
   Irreversible Δf / residual ΔW → passivation-layer evolution

Co-anion dictates the interphase

OTf^-	thickest, most porous, solvent-coupled film (h ≈ 155 nm); highest CE ~86%
BH_4^-	intermediate, most permeable network (ε ≈ 52 nm); cumulative layer
$HMDS^-$	thinnest, densest, most rigid deposit (h ≈ 90 nm); stable passivation

Same read-outs apply directly to Cu, Ni and Zn baths: rate, efficiency, porosity and additive uptake, all in situ.

FIGURES: Fig. 3, Fig. 4, Fig. 5 & Fig. 6 — Yang et al., J. Mater. Chem. A 14 (2026) 25741

Metal electrodeposition followed by EQCM(-D)

Beyond mass: EQCM-D adds dissipation (ΔD) across overtones, turning the balance into an in-situ probe of **viscoelasticity, porosity and solvent coupling** of the growing deposit.

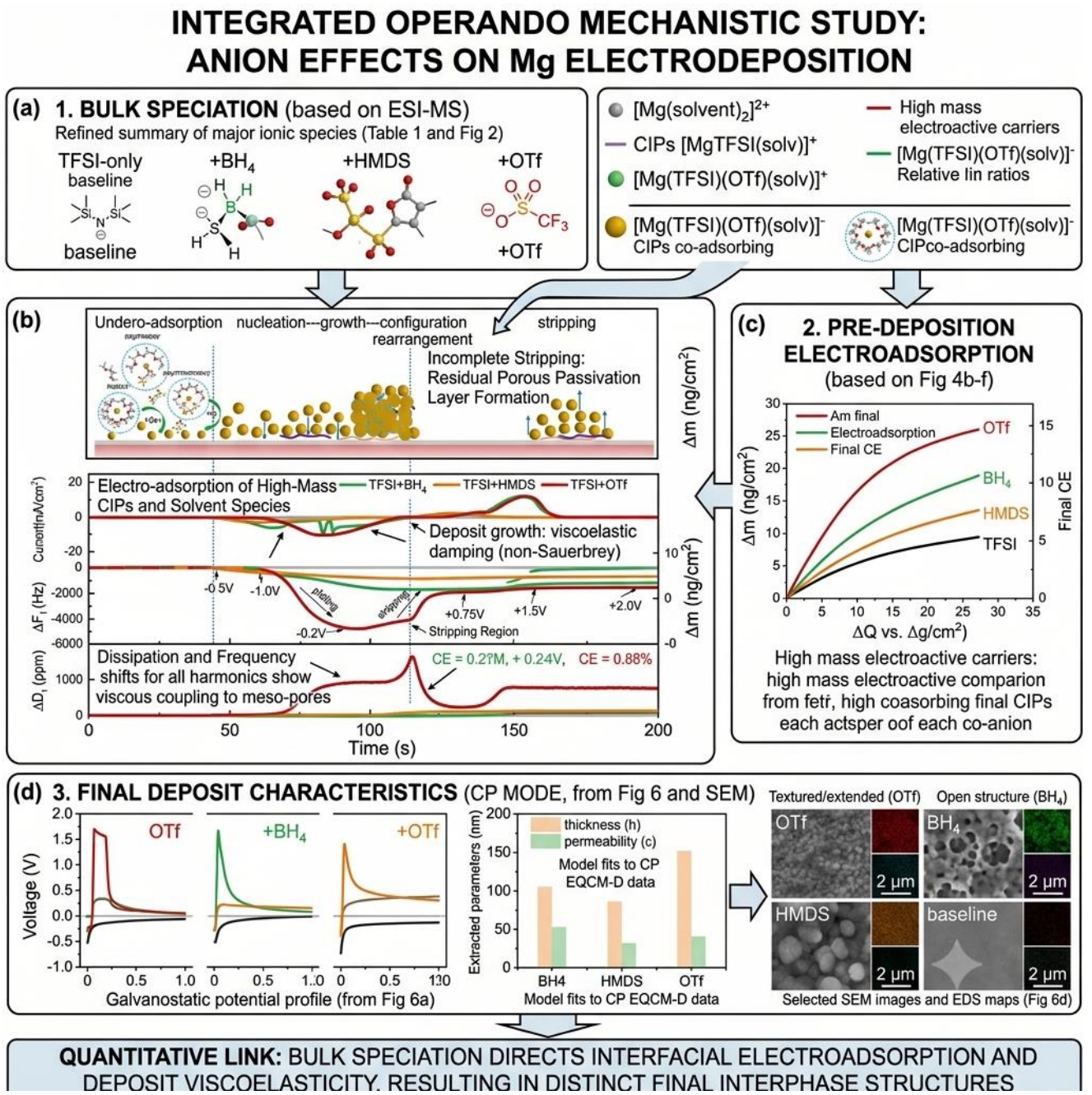

KEY TAKEAWAYS

EQCM turns the deposition current into mass — and mass into mechanism

Kinetics
dΔm/dt vs. E (massograms) reads deposition free of the HER current.

Efficiency
Δm vs. ΔQ → M/z benchmarks real yield against Faraday's law.

Nucleation
HER-free mass transient recovers true 2D/3D growth behaviour.

Alloys/additives
Resolves co-deposited phases, additive & surfactant incorporation.

Viscoelasticity
EQCM-D dissipation exposes porous vs. rigid, solvent-coupled films.

Cross-validate
Pair with SEM/XRD/EDS to tie mass signatures to structure.

Sources: Díaz-Arista 2006 · Hu 2023 · Nakayama 2025 · Yang 2026 · Zong 2025

ELECTROCHEMICAL QUARTZ CRYSTAL MICROBALANCE

EQCM in Corrosion Science

Tracking mass changes at the metal–electrolyte interface in real time

Section: Corrosion

~ 20 min

Built on: Petrunin et al. 2020 · Parasinska et al. 2024 · Yurt & Solmaz 2020 · Broda & Inzelt 2020 · Walsh 2026

Why EQCM for corrosion?

- A resonating AT-cut quartz crystal weighs the electrode in situ — down to nanograms per cm².
- Sauerbrey law: a frequency drop means a mass gain on the surface.
- The crystal is also the working electrode — gravimetry and electrochemistry recorded at once.
- This is what charge alone cannot give: it separates film growth from metal dissolution.
- Practically inertia-free response (µs) → true real-time monitoring.

SAUERBREY EQUATION

$$\Delta f = -(2 / \rho q v q) \cdot f_0^2 \cdot \Delta m$$

Δf: frequency shift · Δm: mass change · f0: base frequency

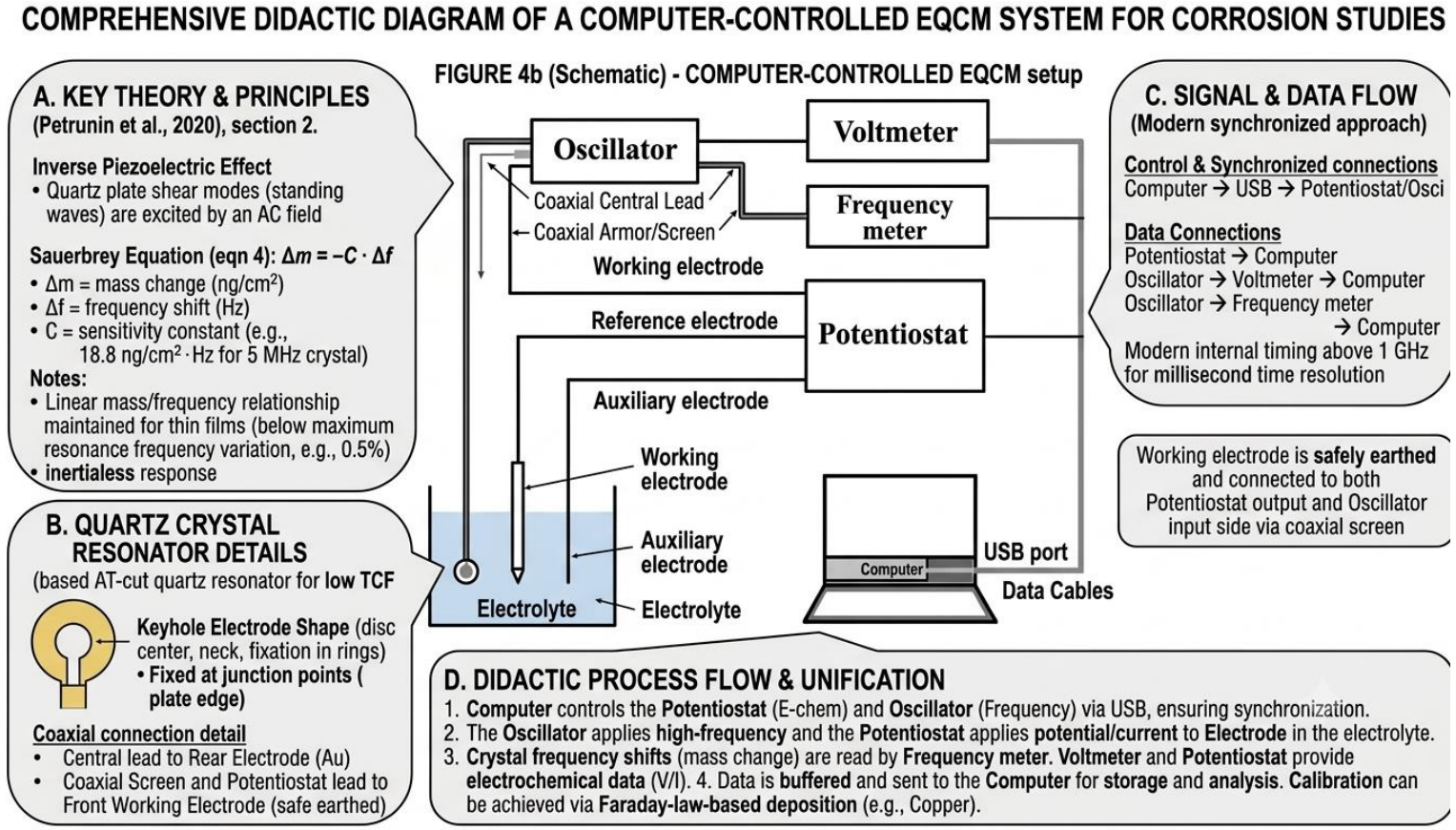

Petrunin, Gladkikh, Maleeva et al., Int. J. Corros. Scale Inhib. 9 (2020) 92–117.

What EQCM reveals in corrosion

1	**Passive film growth, dissolution & breakdown**	Follow oxide layers form, thin, and lose conductivity in real time.
2	**Instantaneous corrosion rates from Δm/Δt**	Turn the mass–time slope directly into a corrosion rate.
3	**Pitting & aggressive ions (Cl−)**	Detect chloride-driven acceleration and local attack.
4	**Inhibitor adsorption & protective films**	Weigh inhibitor uptake and barrier build-up on the metal.
5	**Case study — copper in chloride media**	Coupled DEIS + EQCM on Cu in 0.1 M NaCl.

Passive film growth & dissolution

- Passive films grow as O^{2-} / OH^- incorporate into the surface → electrode mass rises.
- At the same time metal ions dissolve at the film/solution interface → mass falls.
- Comparing measured Δm with charge q separates the two competing reactions.
- The growth fraction R_g tells how much oxidised metal stays in the film vs. dissolves.
- For iron in borate buffer, EQCM + chronoamperometry resolved a primary film only a few monolayers thick (~1 nm).

$$\Delta m_I = qM_m/nF \qquad R_g = (M_m + nF\cdot\Delta m/q)/(M_m + \nu M_0)$$

Charge–mass ratio → oxide-growth fraction

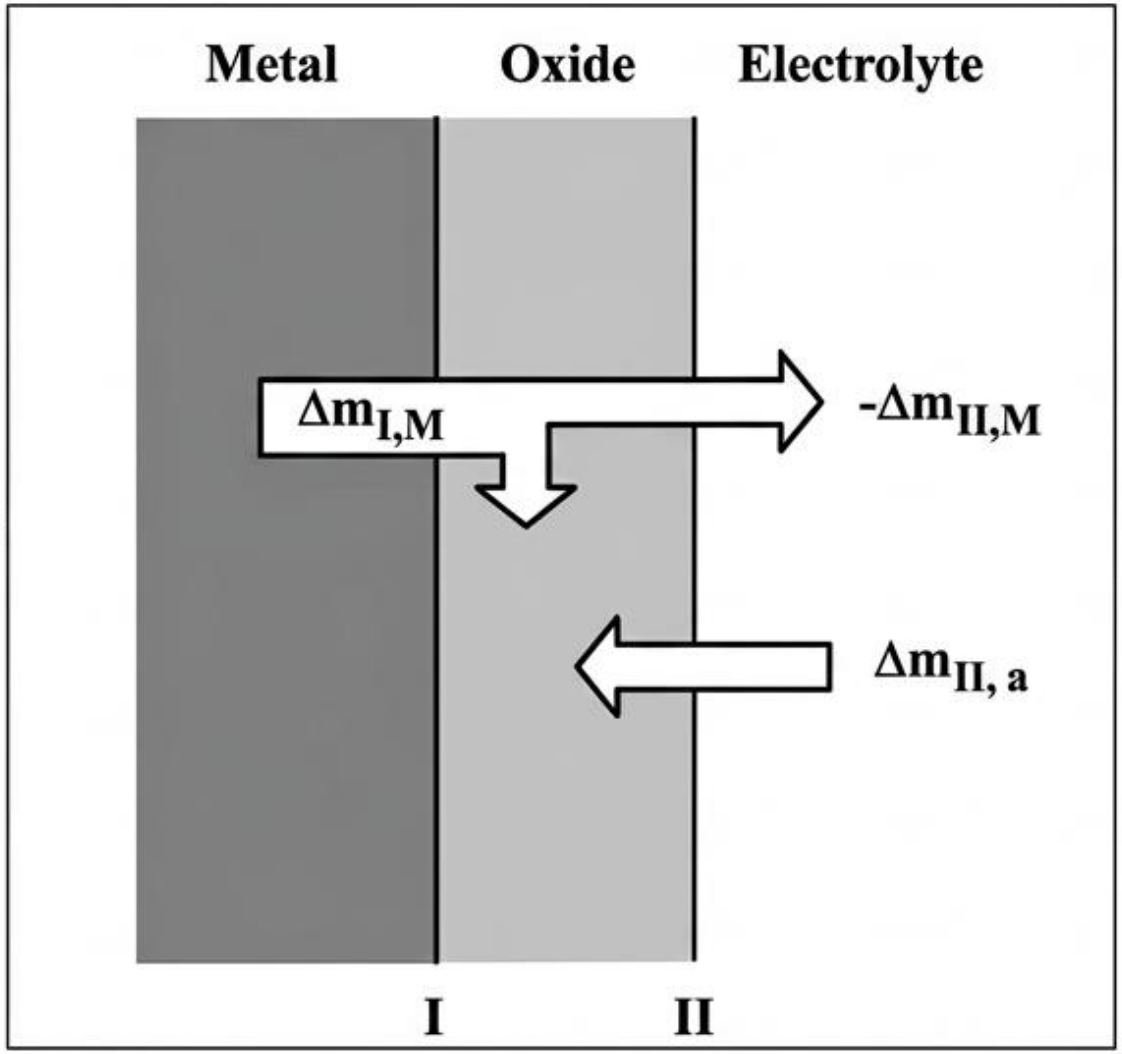

Petrunin et al. 2020, §6.4 · Fe passivation after Marshakov et al. (ref. 37).

Watching a film transform & break down

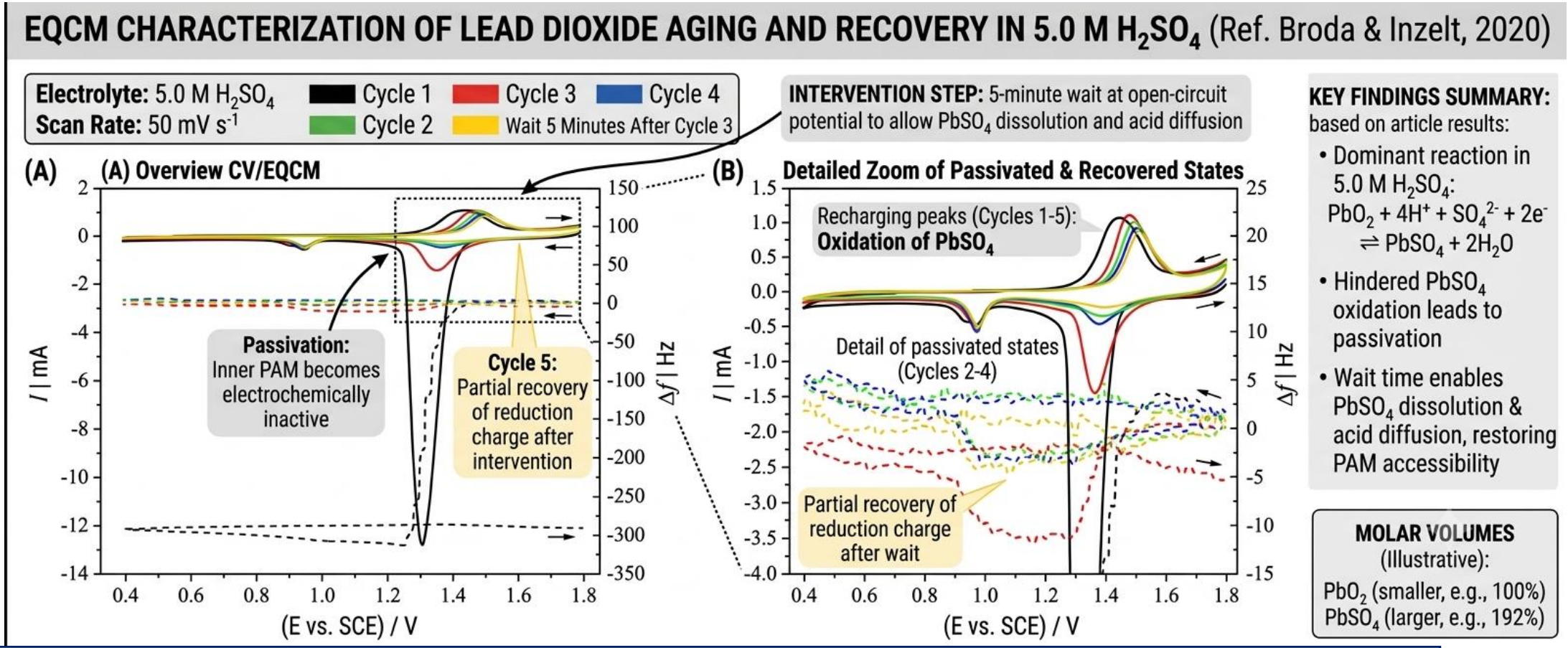

- Case: β-PbO_2 oxide films in H_2SO_4 — simultaneous cyclic voltammetry + Δf, cycle by cycle.
- The effective molar mass from Δm/Δq fingerprints each step of the transformation.the inner oxide.
- Reduction converts $PbO_2 \rightarrow PbSO_4$; a non-conductive, less dense sulfate layer covers the oxide.
- That layer temporarily isolates the film — a real-time picture of conductive-film breakdown & re-activation.
- A short open-circuit wait lets acid diffuse back in and re-activates the inner oxide.

Instantaneous corrosion rate from Δm/Δt

$rate = \Delta m/\Delta t\ (\mu g\ cm^{-2}\ min^{-1})$ $i_a = nF\cdot(dm/dt)/M$

Independent, uninterrupted in-situ rate

DIDACTIC Infographic Table: EQCM-Based Corrosion Analysis of Copper Electrodes with Phosphonic Acid Monolayers

(Data at 25°C in 0.1 M H_2SO_4)

METHOD: Electrochemical Crystal Microbalance (EQCM) with Sauerbrey Equation

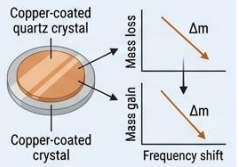

Δf = the mass gaint of balarnes Δm (− (mass gain or loss) — mass gain or loss and corrosiors from frequency =t frequenty of frequency shift.

Corrosion Rate derived from Δm and the conrosion sutan data of at me·adurt places (s ftatnred to as):

$$\Delta f = \frac{-C_f \cdot \Delta m}{R_h}$$

(Cf: sensitivity factor)

$$\text{Corrosion Rate} = \frac{\Delta m}{\text{Electrode Area}}$$

Surface Modification	Immersion Time (h)	Frequency Shift, Δf (Hz cm^{-2})	Electrode Mass Loss, Δm (μg cm^{-2})	Corrosion Rate (μg cm^{-2} min^{-1})
Unmodified Copper (–)	6	8993	−158.89	0.441
	12	15056	−266.01	0.369
	24	28892	−510.46	0.354
	48	85998	−1329.52	0.462
AHP 1-Aminohexyl phosphonic acid	6	1855	−32.77	0.091
	12	2635	−46.55	0.065
	24	3658	−64.63	0.045
	48	5609	−99.10	0.034
BDPA 1,4-Butanedi phosphonic acid	6	5367	−94.82	0.263
	12	11229	−198.39	0.275
	24	25330	−447.53	0.311
	48	75251	−1518.78	0.527
ADBP 1-amino-1,3-dimethylbutyl phosphonic acid	6	7065	−124.82	0.344
	12	12826	−226.61	0.315
	24	26718	−472.05	0.328
	48	57474	−1015.44	0.353

Best Protection Efficiency

Notice: Accelerated Corrosion Rate at 48h (0.527), indicating breakdown of protective SAM

ranking key 1 AHP 2 BDPA 3 ADBP

KEY FINDINGS SUMMARY: ORDER OF PROTECTION EFFICIENCY

1 **AHP** (1-aminohexyl...)

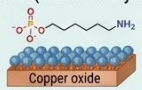

Denses well-packed monolayers (Rank 1)

2 **BDPA** (1,4-butane...)

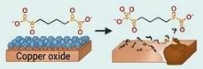

Diphosphonic structure (symmetric) – initial protection, followed by breakdown (Rank 2, with detailed note about at 48h (0.527), indicating breakdown of protective SAM)

3 **ADBP** (1-amino-1...

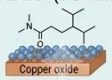

Branched chain structure – stable but less densely packed (Rank 3)

Source: Petrunin et al., (2020). DOI: 10.1142/S0218625X1950166X

EQCM Characterization of Acid Corrosion Protection on Copper with Phosphonic Acid Monolayers (Yurt & Solmaz, 2020)

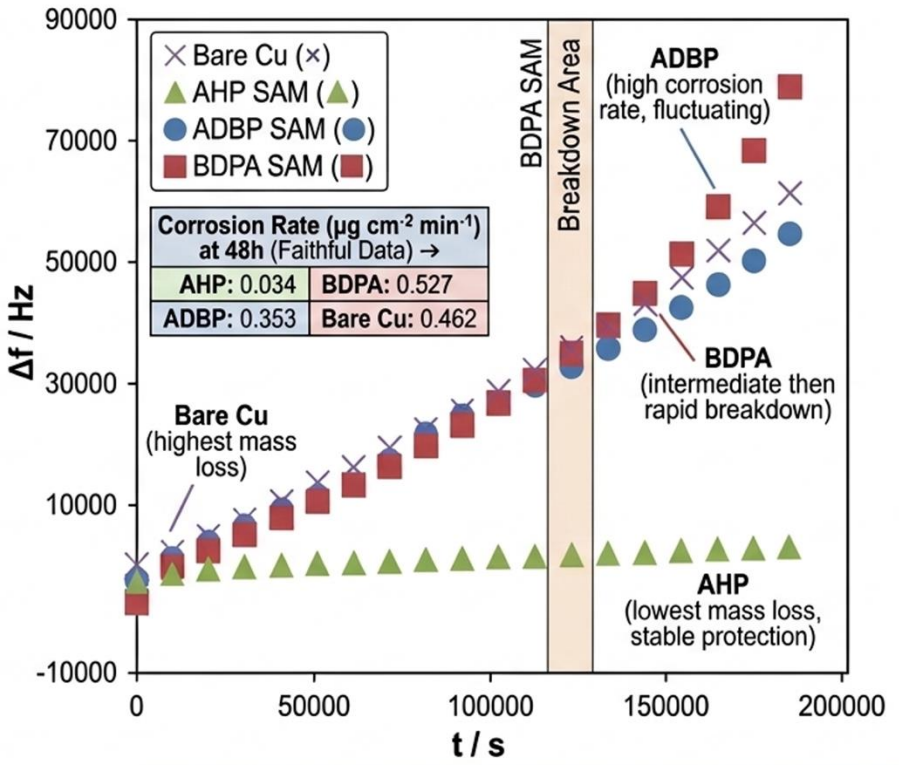

INTERPRETATION OF PROTECTIVE SAM ABILITY

AHP SAM (▲)

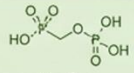

BEST PROTECTION

- Stable monolayer prevents Cu dissolution
- Barrier properties are optimal
- Low corrosion rate

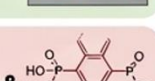

BDPA SAM (■)

SAM BREAKDOWN & SOLUBLE COMPLEXATION

- Initially intermediate
- Breakthrough after ~36 hours (Ref: text 36 h breakdown)
- Reasons: breakdown + soluble Cu(II) complexes form (complexation activated corrosion)
- Polydentate nature increases solubility

ADBP SAM (●)

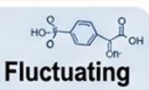

HIGH CORROSION, Fluctuating

- High initial rate
- Fluctuations
- Defects in monolayer (Ref: text defective sites), incomplete coverage

Overall Protective Efficiency Rank: AHP/Cu > BDPA/Cu > ADBP/Cu > Bare Cu (Faithfully based on detailed text)

Yurt & Solmaz, Surf. Rev. Lett. 27 (2020) 1950166.

Inhibitor adsorption in real time

- The nanogram sensitivity of EQCM tracks inhibitor uptake as it happens.
- Adsorption isotherms (e.g. Frumkin) come from EQCM combined with ellipsometry.
- Benzotriazole on Cu: after injection the mass (frequency) locks in → a stable protective layer forms at once.
- Sodium folate: mass tracks the bare-metal case on a smaller scale → weak, non-lasting interaction.
- The contrast is read straight from the frequency channel.

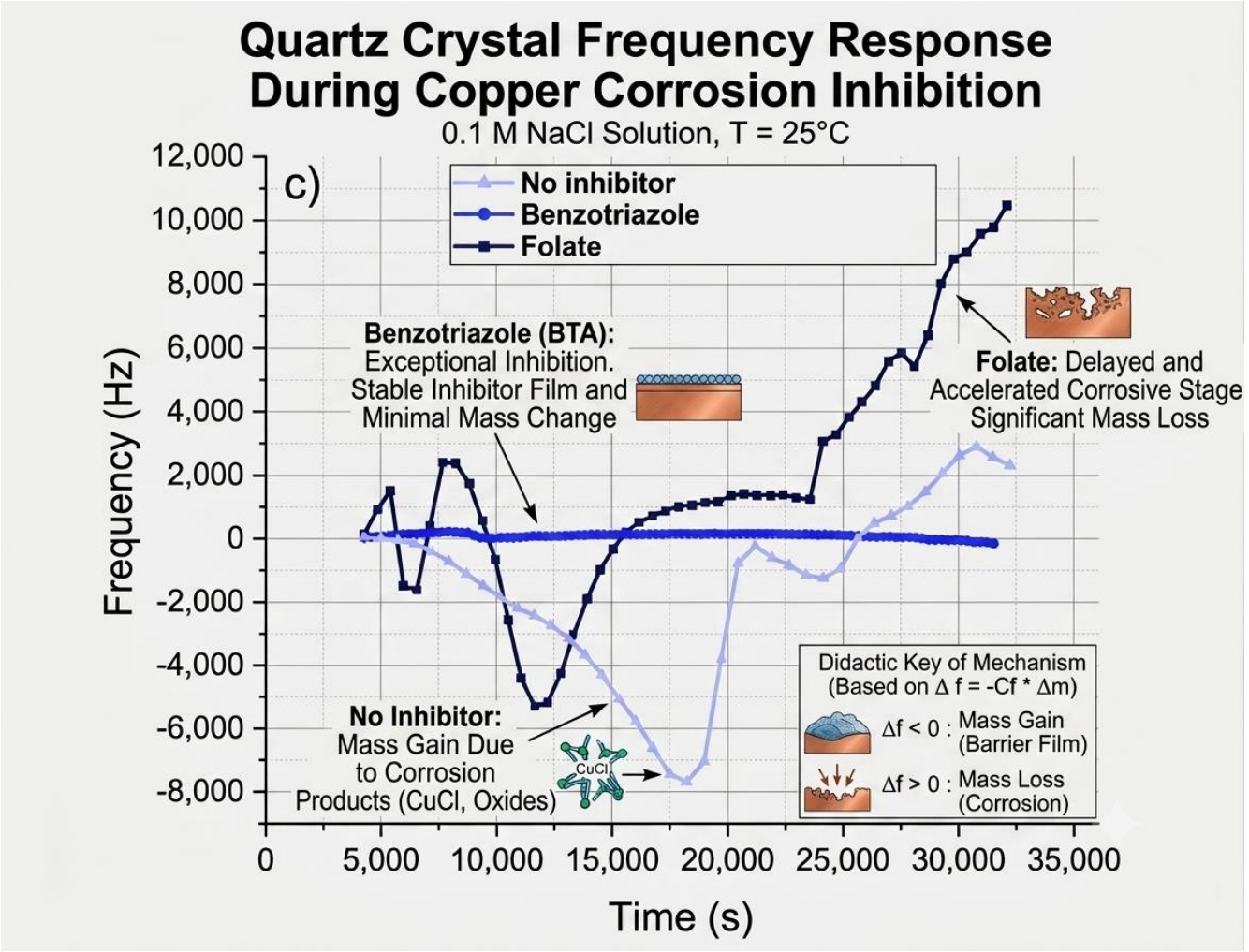

Quartz-crystal frequency (mass) vs. immersion time: benzotriazole holds Δf constant (protected), whereas folate and the blank keep drifting.

Parasinska et al., J. Mater. Manuf. 3(1) (2024) 8–16.

Take-home messages

Nanogram, in situ mass tracking

EQCM weighs the electrode as it corrodes — charge alone can't do this.

Film growth vs. dissolution, resolved

Δm + q separate oxide formation from metal loss; rates come from Δm/Δt.

Chloride & inhibitors, quantified

Detects Cl−-driven acceleration and barrier-film formation directly.

Strongest in combination

Pair with EIS/DEIS, ellipsometry, XPS, AFM for full mechanism.

References

- M.A. Petrunin, N.A. Gladkikh, M.A. Maleeva, T.A. Yurasova, E.V. Terekhova, L.B. Maksaeva. Application of the quartz crystal microbalance technique in corrosion studies. A review. Int. J. Corros. Scale Inhib. 9 (2020) 92–117.
- D. Parasinska, H. Kwiatkowski, P. Slepski. Application of quartz crystal microbalance and dynamic impedance spectroscopy to the study of copper corrosion inhibitors. J. Mater. Manuf. 3(1) (2024) 8–16.
- A. Yurt, E. Solmaz. Phosphonic acid monolayers for corrosion protection of copper: EQCM and EIS investigations. Surf. Rev. Lett. 27(6) (2020) 1950166.
- B. Broda, G. Inzelt. Investigation of the electrochemical behaviour of lead dioxide in aqueous sulfuric acid solutions by the in situ EQCM technique. J. Solid State Electrochem. 24 (2020) 1–10.
- F.C. Walsh. Corrosion, electrodeposition and tribology: reporting guidelines. Trans. IMF 104(2) (2026) 64–70.

EQCM-D Applied to Polymers

Gravimetric and viscoelastic insights into polymer films:
water uptake, ion exchange, and mechanical stability

Based on:

- Benedetti & Torresi, Langmuir 2013, 29, 15589
- Obana et al., Phys. Chem. Chem. Phys. 2021, 23, 12251
- Easley et al., J. Polym. Sci. 2022, 60, 1090

Why QCM-D / EQCM-D for Polymer Films?

High-resolution, real-time mass and rheology at the ng scale

- Converse piezoelectric effect: an AT-cut quartz crystal oscillates under an alternating potential; frequency (f) and dissipation (D) are tracked at multiple overtones
- Sensitivity down to ~4.4–17.7 ng cm^{-2} Hz^{-1} (5 MHz sensors) with >100 pts/s — molecular-scale access to mass transport
- **Δf → mass changes; ΔD → softening/stiffening (viscoelasticity)**
- Polymers swell and have a viscous component → dissipation monitoring is essential
- Coupled with electrochemistry (EQCM-D): correlates ion/solvent exchange and rheological changes with redox state
- Applications: film growth, sorption, swelling, ion exchange, gas sensing, energy storage electrodes

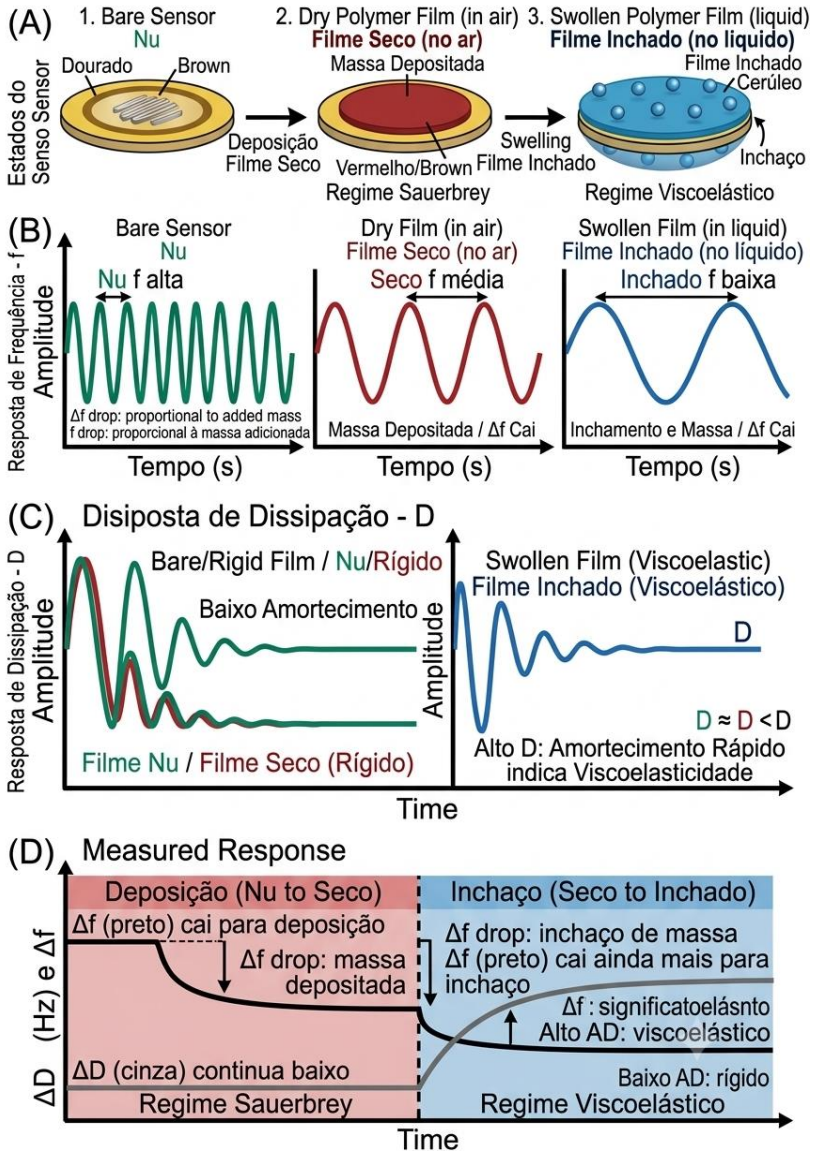

Modeling the QCM-D Response

Choosing between Sauerbrey and viscoelastic (Kelvin–Voigt) models

- **Sauerbrey (rigid films): $\Delta m = -C \cdot \Delta f / n$ — valid when $\Delta D \approx 0$ and overtones overlap**
  - Criterion: $|\Delta D_n/(\Delta f_n/n)| \ll 4\times10^{-7}\ Hz^{-1}$ → Sauerbrey may be used
- **Kelvin–Voigt (viscoelastic films): spring + dashpot in parallel; $G^* = G' + iG'' = \mu f + i2\pi f \eta f$**
  - Use when $\Delta D > 0$ and overtones spread; yields μf (elastic shear modulus) and ηf (shear viscosity)
  - Fit ≥ 3 overtones (exclude the fundamental) for a quality fit
- Extended Voigt: frequency-dependent moduli (e.g., polyelectrolyte multilayers)
- Hydrodynamic model: porous/particulate films in liquid

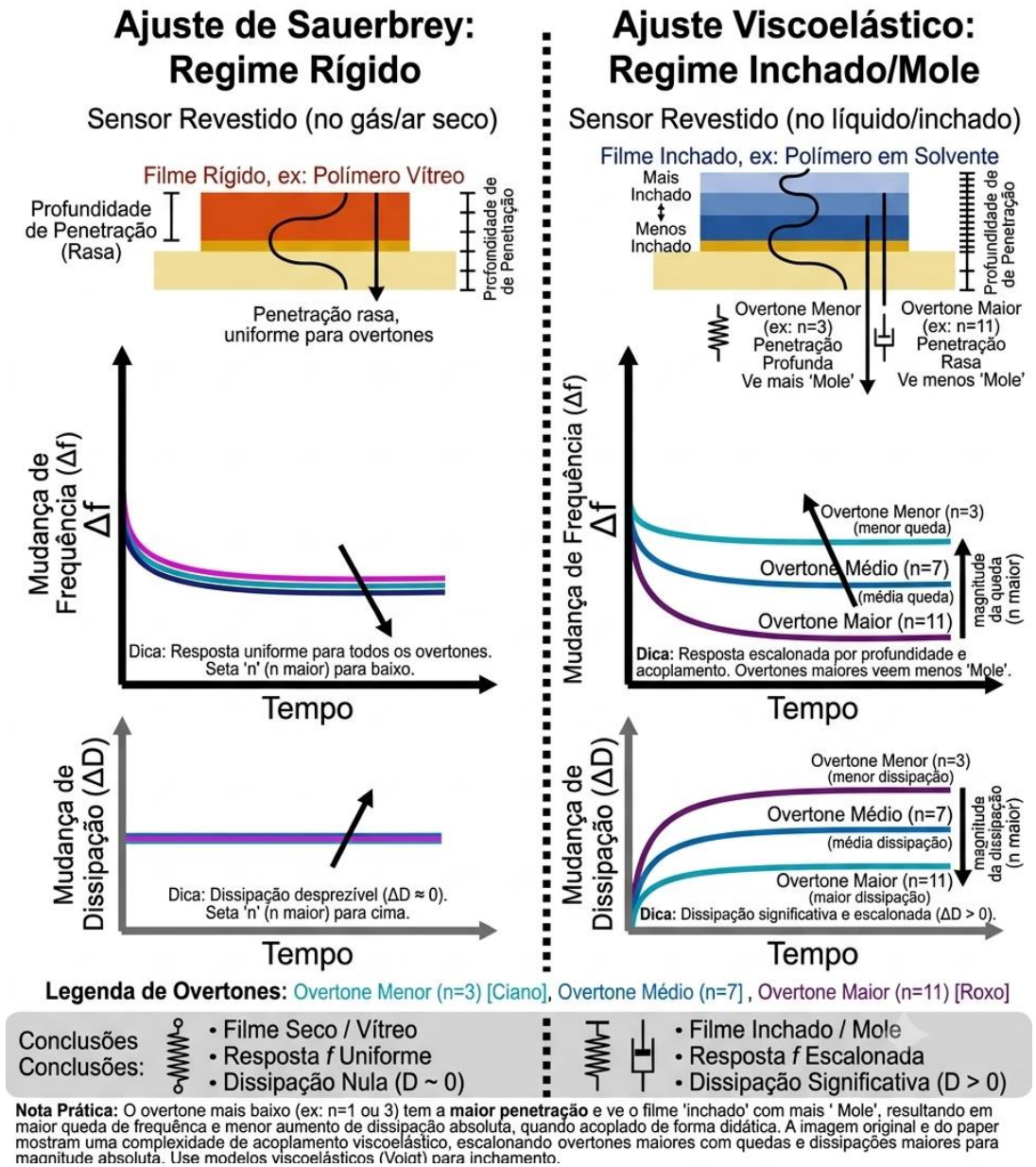

Case 1 — Water Uptake by Poly(ionic liquid) Thin Films

$PDDATf_2N$ / $Pyr_{1.4}Tf_2N$ / $LiTf_2N$ spin-coated films under dry ↔ wet N_2 flow

- Thin films (50–70 µg cm^{-2}) spin-coated on 5 MHz Pt quartz sensors; humidity set by saturated salt solutions (11–98%)
- Switching dry → wet N_2: f decreases and D increases, stabilizing in ~150 s; fully reversible on switching back
- **ΔD changes are significant (>5% relative to Δf) → Kelvin–Voigt modeling required to separate mass from viscoelastic effects**
- Model outputs: mass of absorbed water vs. time + µf and ηf for each composition

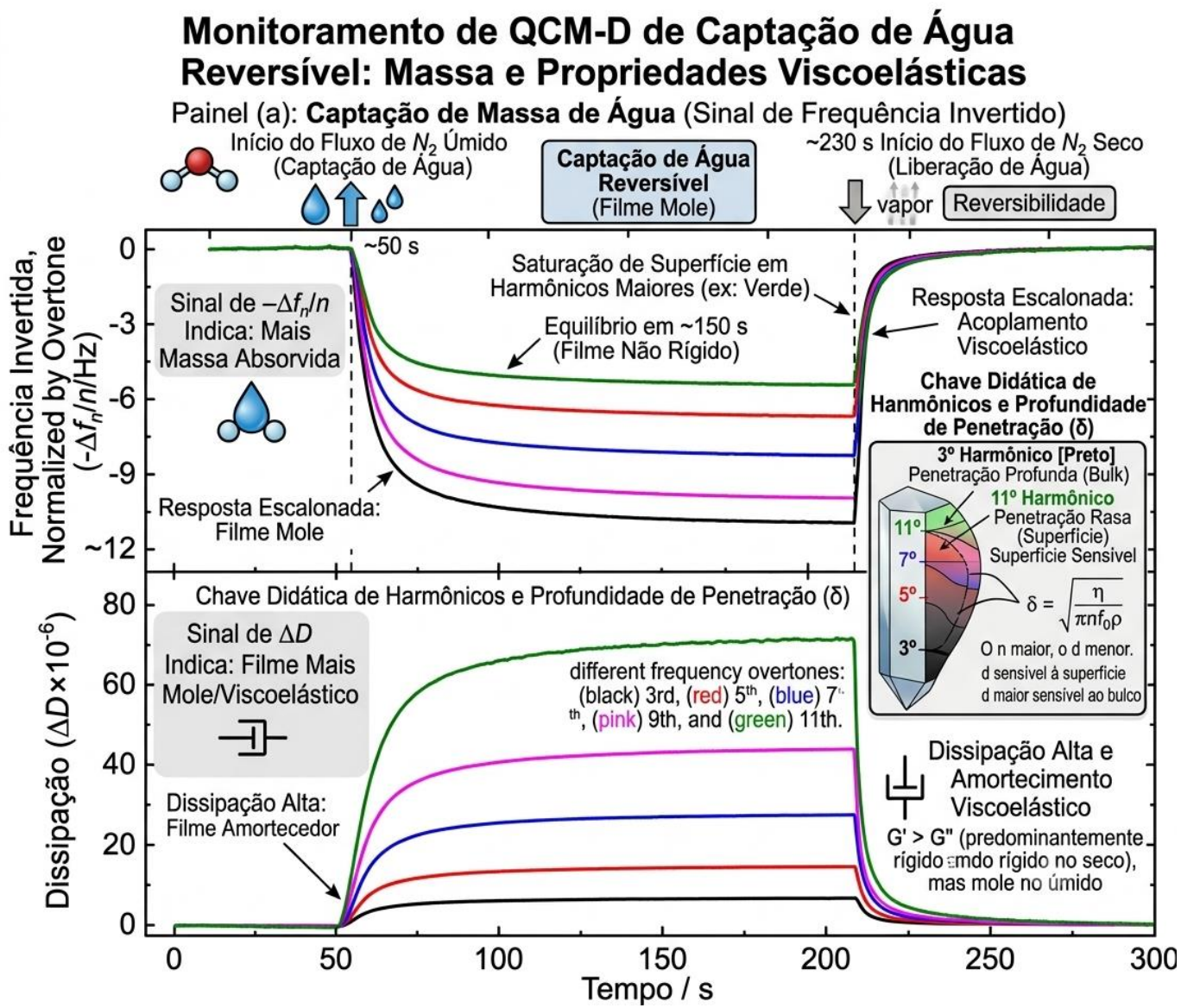

Case 1 — Rheology: the IL Acts as a Plasticizer

Viscoelastic parameters from the Kelvin–Voigt fit

- **Dry films: μf drops from 12 GPa (pure POIL) to 0.31 GPa with 33% IL and 0.14 GPa at 50% IL → IL strongly reduces rigidity**
- G′/G″ = 57 for pure POIL vs. <10 with IL: all films predominantly rigid, but coupling with the crystal differs
- Hydration: μf decreases for the POIL-only film; effect is minor when IL is present
- Adding 4.8% $LiTf_2N$: μf 0.15 → 8.4 GPa and ηf 0.51 → 44.4 kg m^{-1} s^{-1} (ionic aggregates with Li^+); hydration breaks the aggregates and both drop
- Water uptake at equilibrium: 9.4 → 30.7 mg g^{-1} with Li salt; kinetics follow a pseudo-second-order model

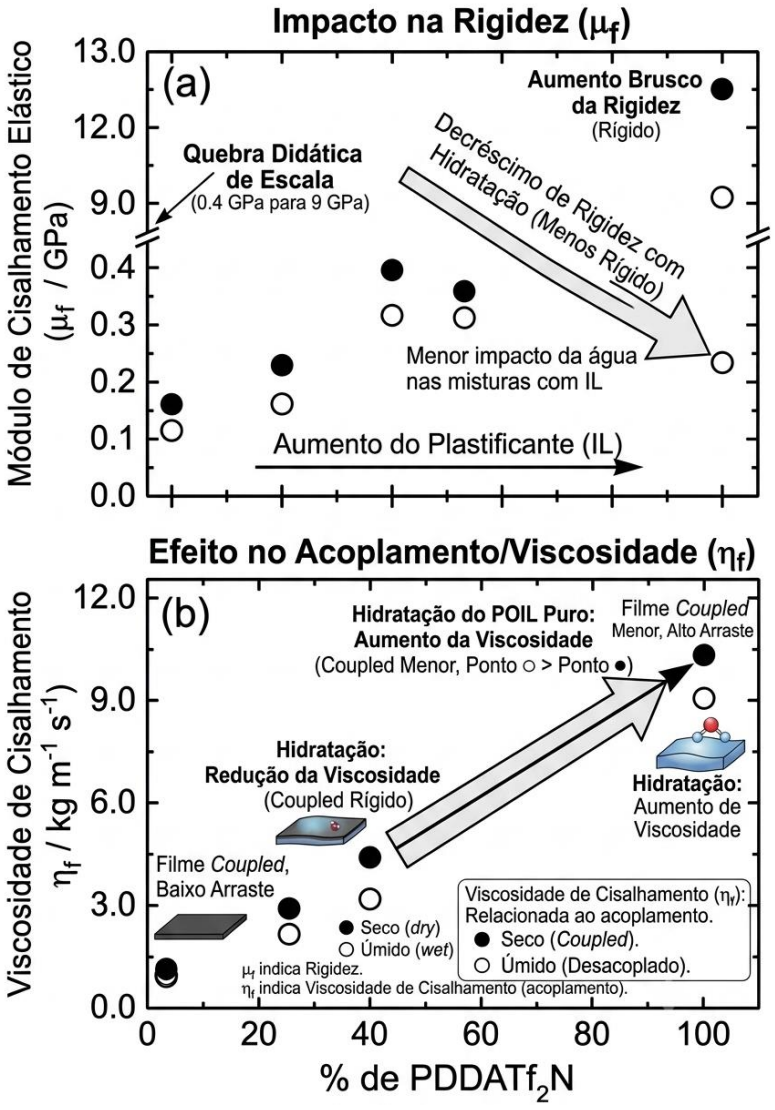

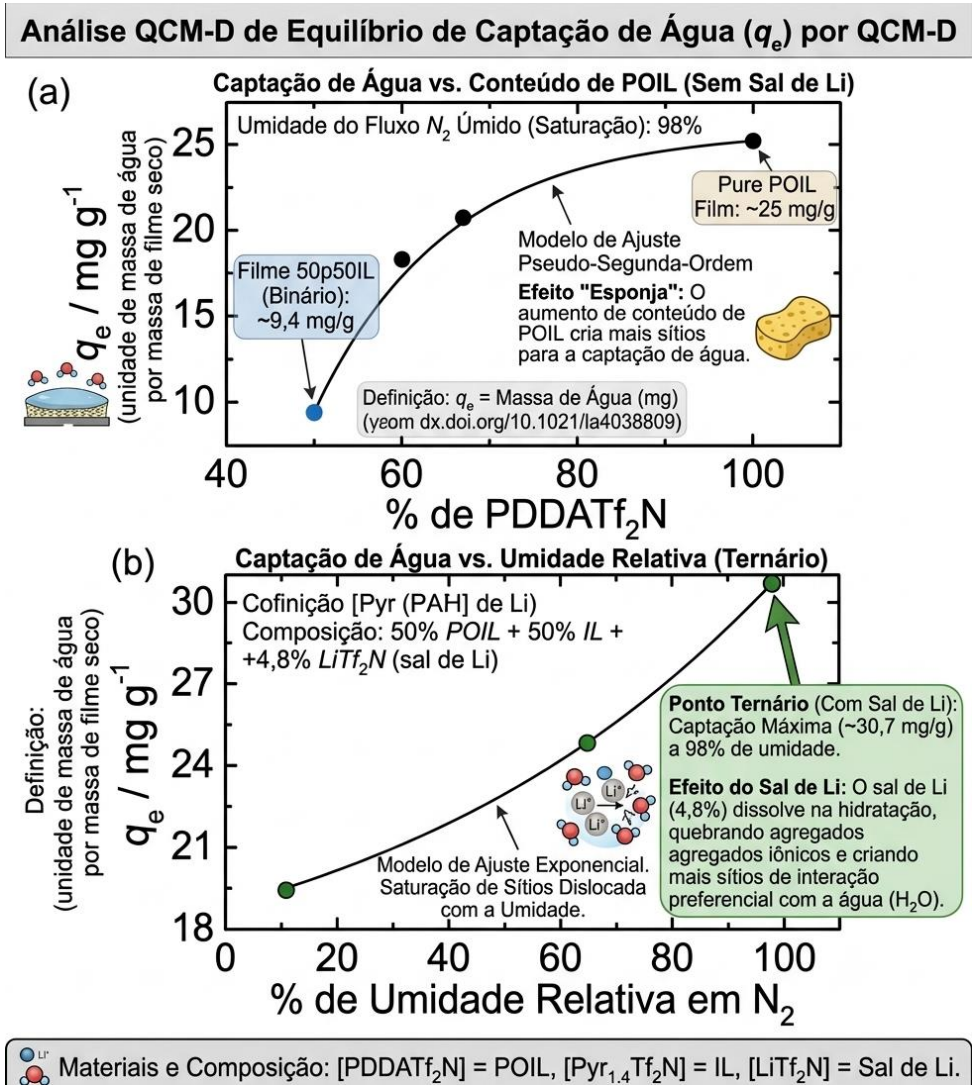

Case 2 — PPy(DBS) in Water-in-Salt Electrolytes (WiSE)

Suppressing volumetric deformation of a conducting polymer

- Dilute LiTFSI (SiWE, 0.1–1.0 mol L^{-1}): overtones do not overlap, large ΔD_n → viscoelastic changes during redox; cation/water ejection on oxidation
- **WiSE (LiTFSI 7.0 mol kg^{-1}): $\Delta f_n/n$ overlap for all overtones and $\Delta D_n < 5\times10^{-6}$ → film stays rigid, Sauerbrey valid**
- Only ~60% free water in the WiSE: altered $Li^+/TFSI^-$ solvation shells
- Charge compensation shifts from mostly cationic (Li^+) exchange to mixed $Li^+/TFSI^-$ exchange with negligible water

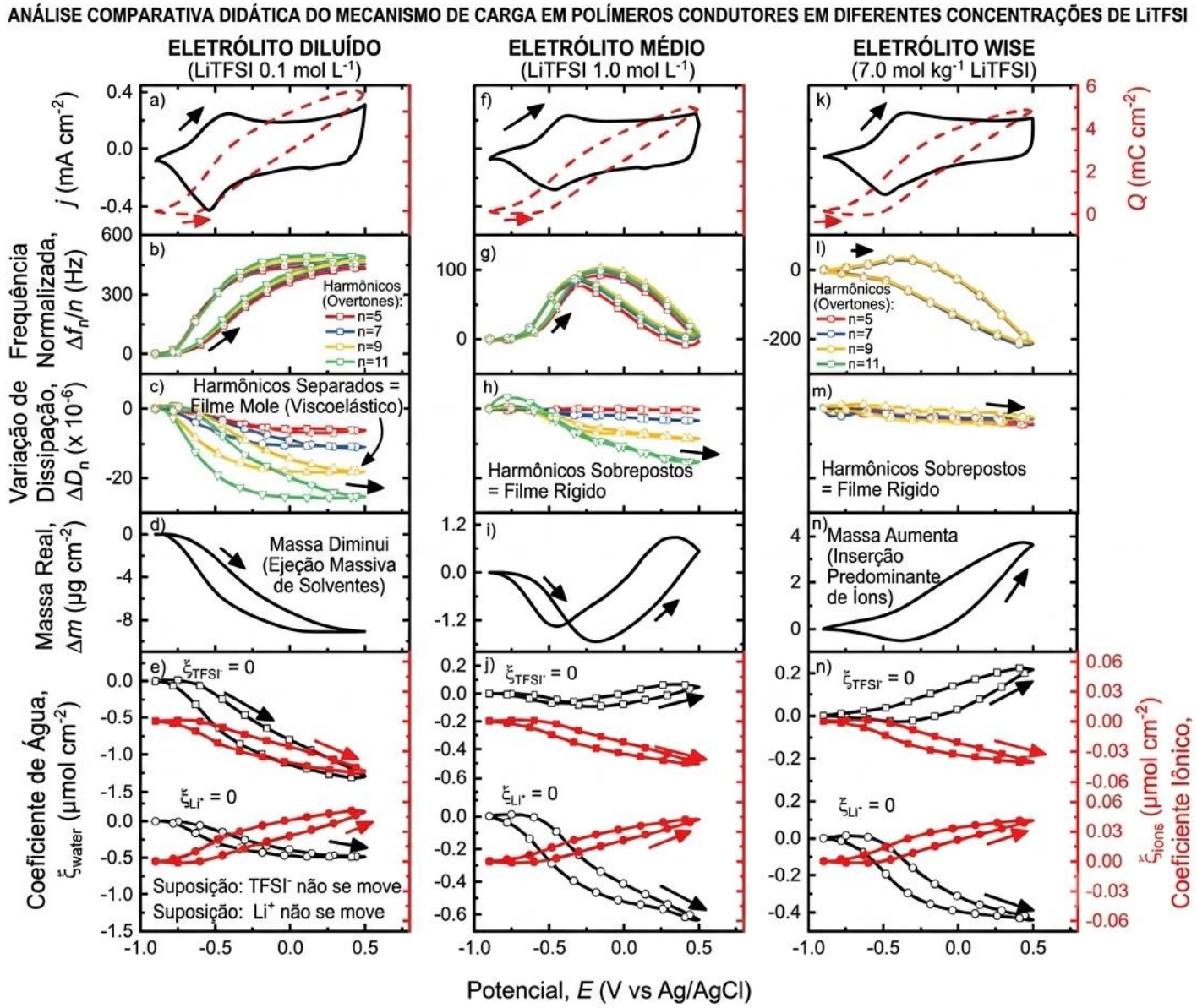

Case 2 — From Rheology to Device Stability

Higher shear modulus in WiSE → less bending → better energy retention

- **Δμ upon oxidation: ~MPa range in SiWEs vs. ~1 GPa for PPy(DBS) in the WiSE — lack of free water to plasticize the chains**
- Thick freestanding films: maximum bending angle decays from ~56° (SiWE) to 3.5° (WiSE); viscosity alone does not explain it
- PPy(DBS)/AC cells: 86% energy retention after 600 cycles in WiSE vs. 76% in 1.0 mol L^{-1} SiWE (~30% less fading)
- EQCM-D + dynamo-voltammetry agree: WiSE hinders mechanical deformation of the polymer

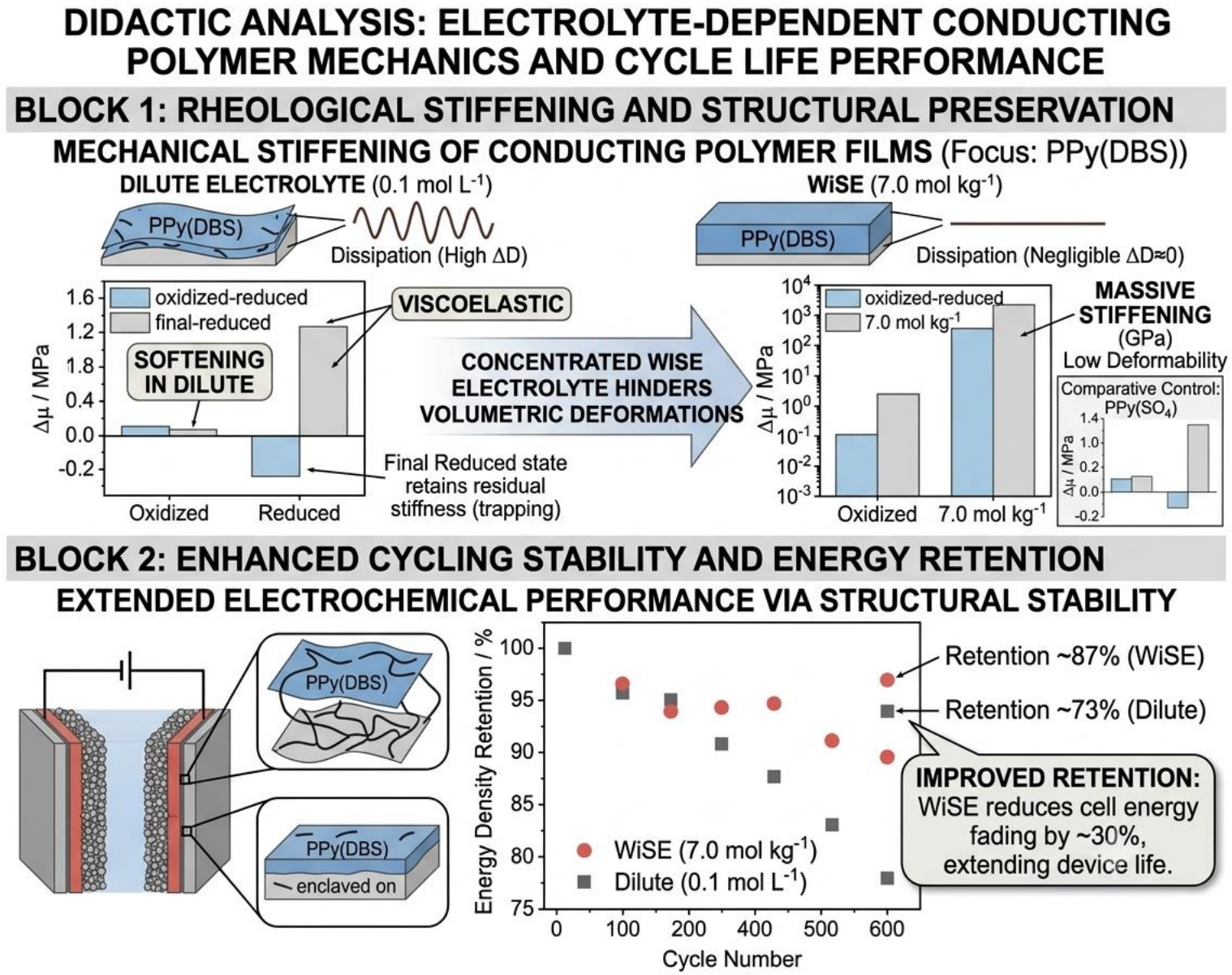

Take-Home Messages

- QCM-D separates mass from rheology: dissipation is the key to polymers, which are rarely rigid
- Model choice matters: Sauerbrey only when $\Delta D \approx 0$ and overtones overlap; otherwise Kelvin–Voigt (μf, ηf, G'/G'')
- Small molecules control mechanics: water plasticizes POIL films; Li^+ builds ionic aggregates that hydration disassembles (Case 1)
- Electrolyte engineering: WiSEs limit water exchange, keep PPy rigid, and extend capacitor cycle life by ~30% (Case 2)
- EQCM-D quantifies coupled electron–ion–solvent transport in redox polymers (Case 3)
- Careful practice (thickness, baselines, bubbles, drift) is what makes the data quantitative

References: Benedetti & Torresi, Langmuir 2013, 29, 15589 • Obana et al., Phys. Chem. Chem. Phys. 2021, 23, 12251 • Easley et al., J. Polym. Sci. 2022, 60, 1090

TECHNIQUES IN ELECTROCHEMISTRY · 20 MIN

EQCM & QCM-D in Bioelectrochemistry

Electrochemical quartz-crystal microbalance with dissipation as a real-time, label-free probe of biological interfaces

SAM platforms | Protein adsorption | Antibody / DNA | Enzyme electrodes | Cells & biofilms

Figures cited on each slide — figure number + source paper

Five faces of EQCM in bioelectrochemistry

01

SAMs on Au crystals

Self-assembled monolayers as tunable biosensing platforms

02

Protein adsorption

Mass + conformational change resolved by dissipation

03

Antibody & DNA

Affinity recognition and hybridization detection

04

Enzyme electrodes

Catalytic activity and bound mass tracked together

05

Cells & biofilms

Adhesion, cytoskeleton and fouling on electrified surfaces

Why dissipation matters: two independent signals

- Δf tracks mass coupled to the sensor (Sauerbrey for thin, rigid films).
- ΔD reports viscoelasticity — soft, hydrated biolayers deviate from Sauerbrey.
- Together they separate dry mass, coupled water and conformation of an adlayer.
- EQCM-D adds a potentiostat: the crystal electrode is driven electrochemically while Δf/ΔD are recorded simultaneously.
- Enables one experiment to link electron transfer, mass change and film mechanics.

Take-home: a rigid protein shifts Δf only; a hydrated biofilm shifts both — QCM-D sees the difference.

Fig. 1 · Dixon 2008

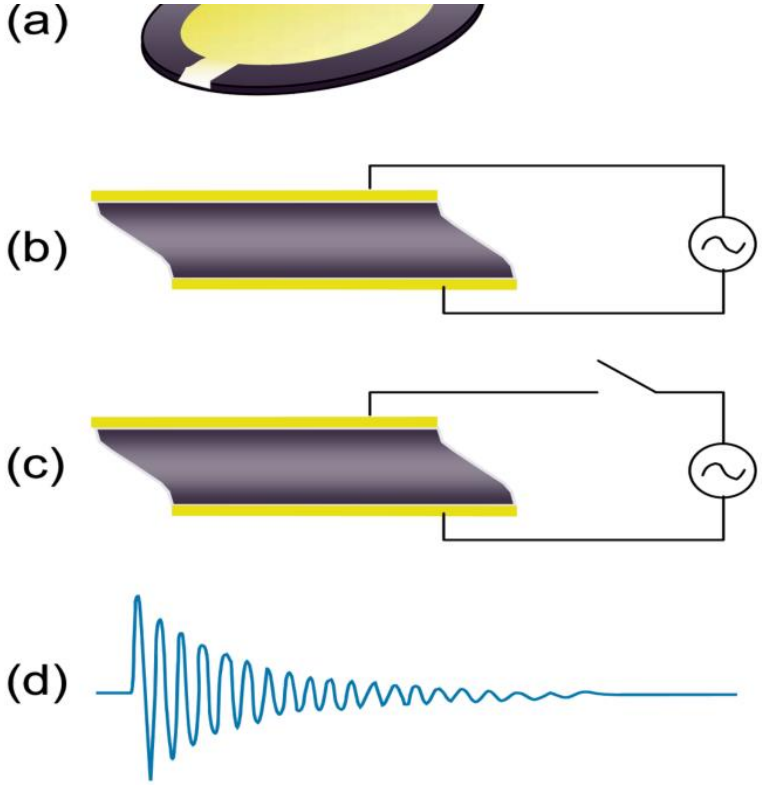

FIGURE 1

. QCM-D components: driven crystal (b), decaying oscillation (d)

SAMs on Au crystals as biosensing platforms

- Thiol self-assembled monolayers chemisorb on the gold electrode, giving a defined, tunable surface.
- Spacer-arm length and lateral density set orientation, packing and how far the biomolecule sits from the transducer.
- Layer-by-layer (glutaraldehyde / lysine) or carboxylate–Ni(II) chemistries graft proteins onto the SAM.
- Same Au/thiol scaffold serves electrochemistry and QCM-D — ideal for EQCM.

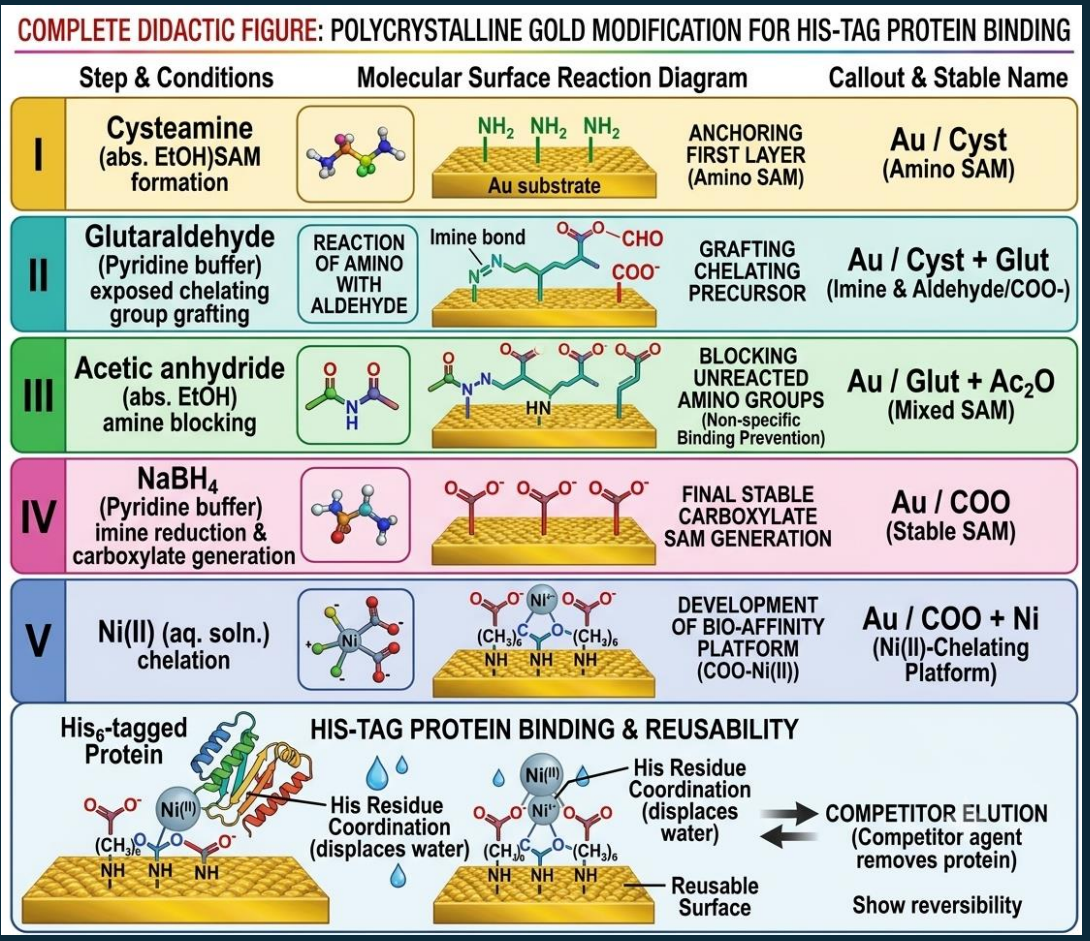

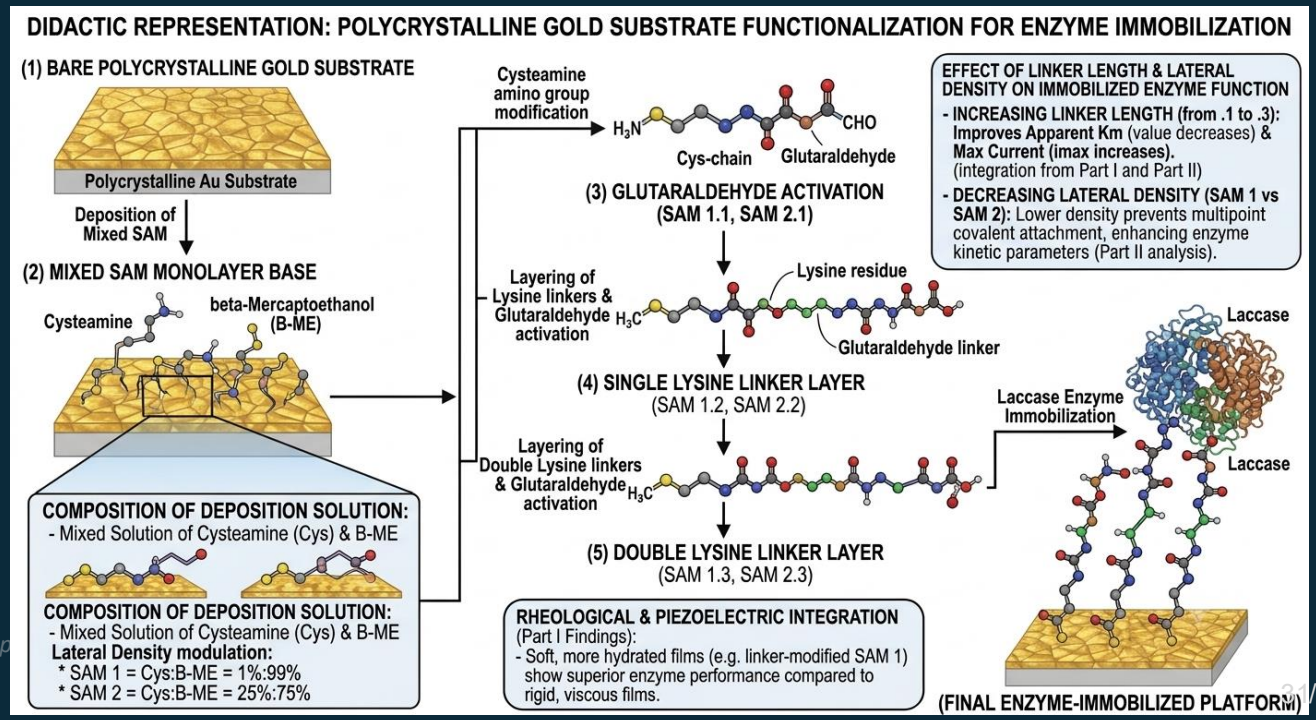

Watching the platform build, layer by layer

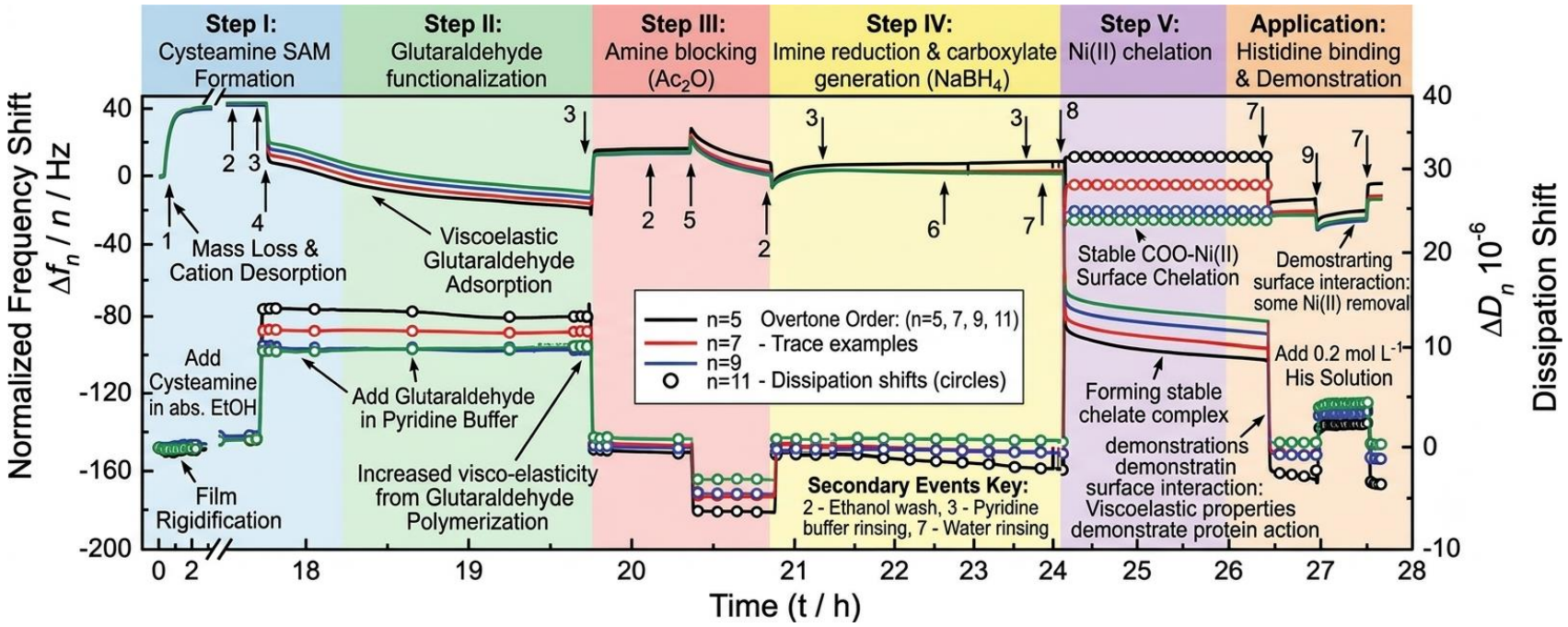

- Each grafting step gives a discrete Δf drop — mass added and quantified in situ.
- Non-spreading overtones + low ΔD confirm an acoustically rigid, well-formed film.
- A viscoelastic 'wet' step that rigidifies on rinsing reveals loosely bound material.
- His-tag capture is confirmed when a competitor (His / imidazole) partially removes Ni(II).

EQCM value: mass, rigidity and reaction completeness — without any label.

Protein adsorption and conformational change

- Rigid protein (HSA): large Δf, negligible ΔD — Sauerbrey mass is reliable.
- Antibody layer: large Δf and large ΔD — extensive coupled water and softness.
- ΔD is the fingerprint of viscoelasticity — size and flexibility raise its weight.
- A buffer rinse that changes signal without net desorption exposes a conformational change (re-orientation / dehydration).
- Comparing QCM-D mass with SPR / ellipsometry quantifies hydration of the film.

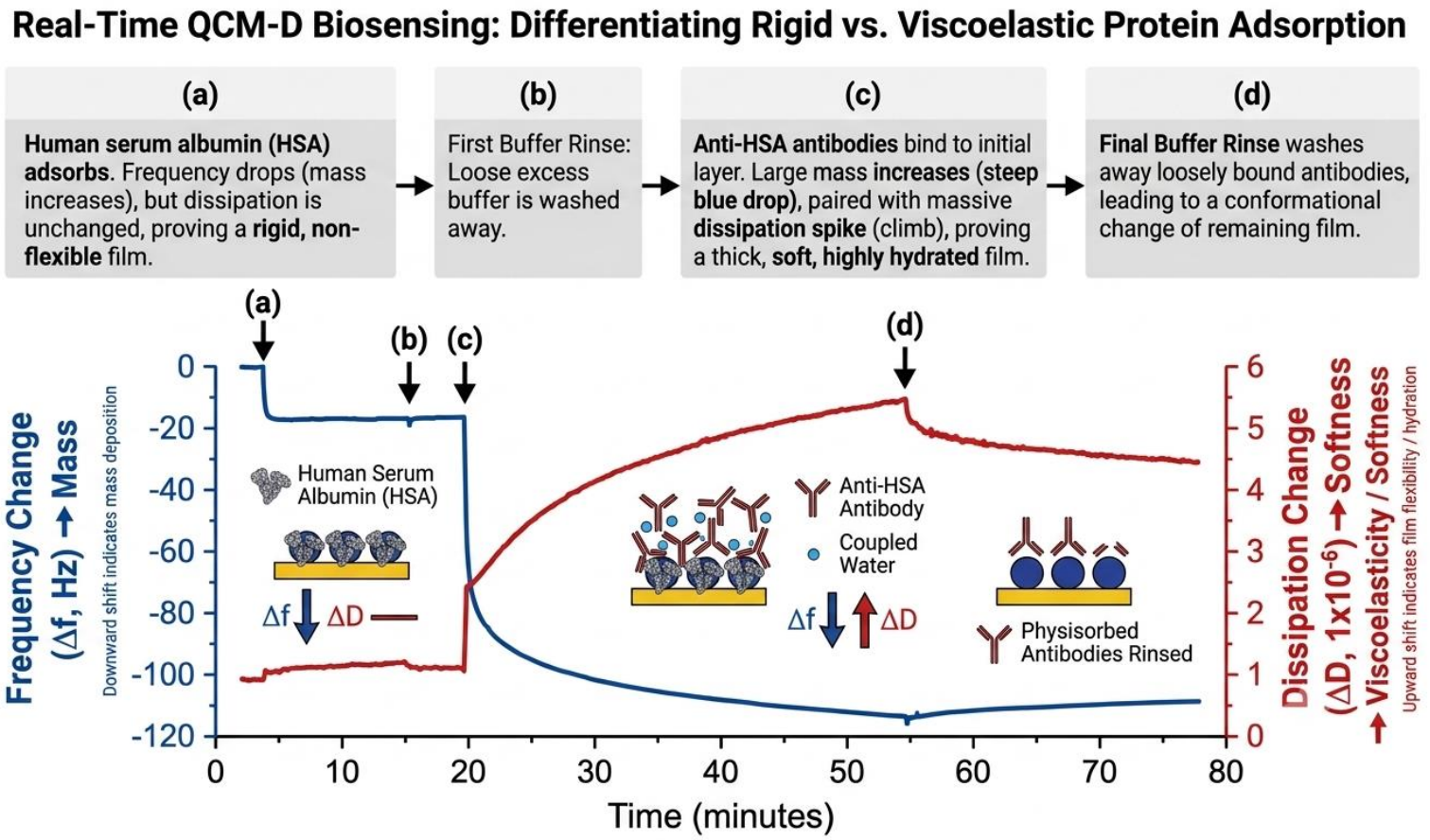

Denaturation on immobilization tracks with film viscosity — softer ≠ more active.

TOPIC 03 · MOLECULAR RECOGNITION

Antibody–antigen recognition & DNA hybridization

AFFINITY CAPTURE

- SAM → biotin → streptavidin → capture antibody builds an oriented recognition layer.
- Antigen / vesicle binding is read as coupled Δf and ΔD — specificity checked against isotype controls.
- Steric crowding of antibodies can lower capture — spacing matters as much as density.

DNA HYBRIDIZATION

- Probe strands immobilized on the crystal; target binding adds mass (Δf) in real time.
- ΔD distinguishes rigid duplex from flexible single strands — a conformational read-out of hybridization.
- Basis for label-free genosensors, ss-/ds-DNA scaffolds and DNA–protein studies.

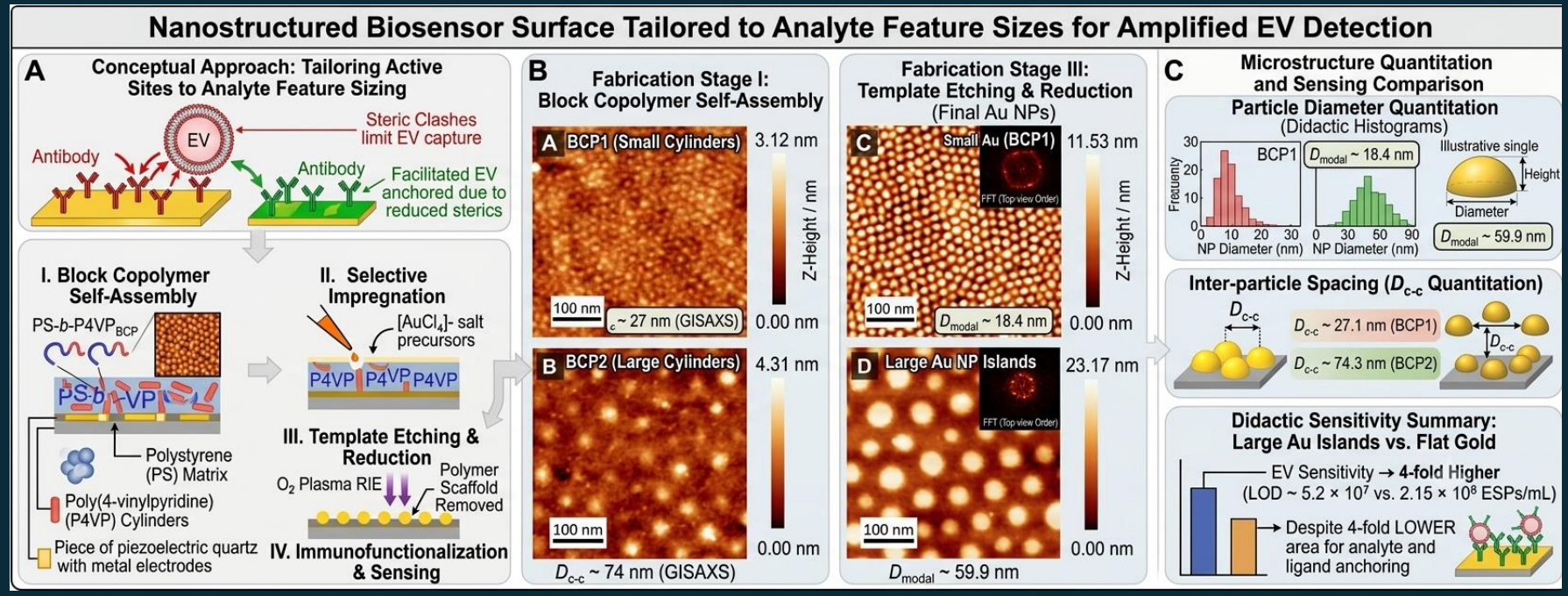

TOPIC 04 · CATALYSIS MEETS GRAVIMETRY

Enzyme electrodes & biofuel cells

- Immobilized laccase oxidizes phenolics; the electroactive product is read by chronoamperometry (activity, imax, Km).
- The same electrode is a QCM-D crystal → bound enzyme mass and film

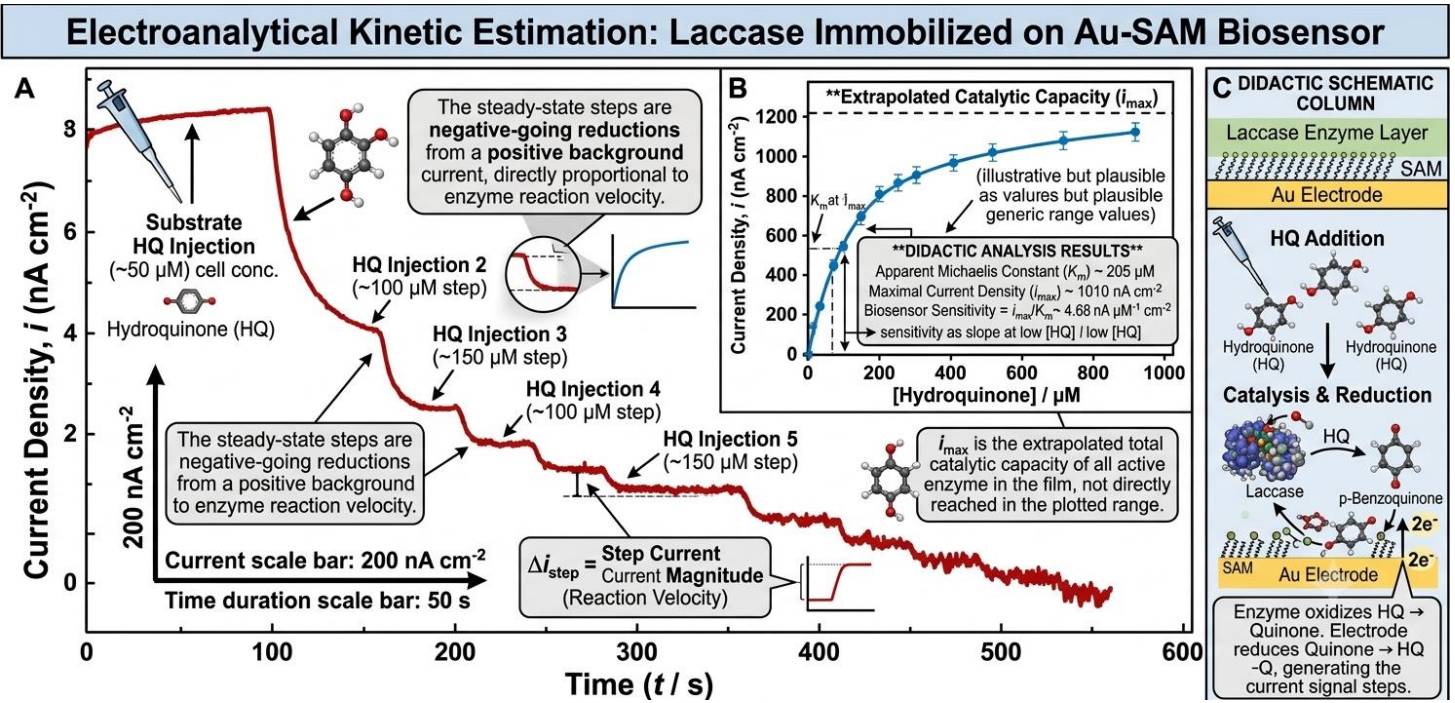

EQCM lesson: bound mass alone can't predict performance — rheology completes the picture.

- Longer linkers lower apparent Km and raise sensitivity: enzyme lifted off the support is better solvated.
- Film viscosity correlates with denaturation; hydration correlates with sensitivity.
- Directly relevant to laccase biocathodes for implantable biofuel cells.

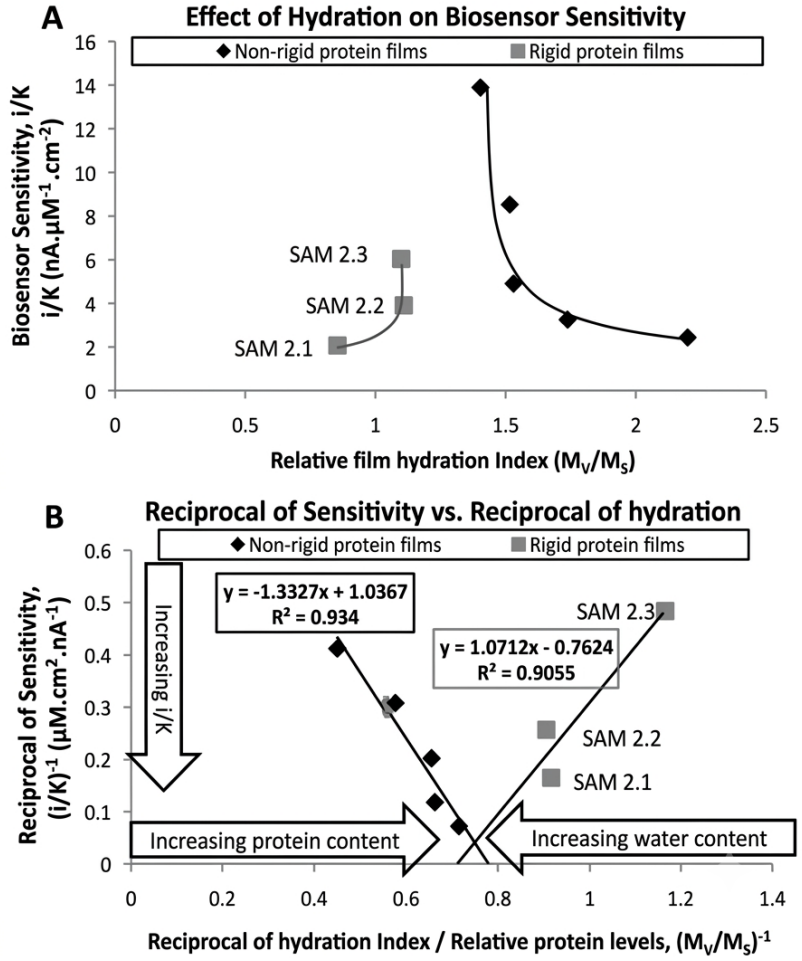

TOPIC 05 · LIVING INTERFACES

Cell adhesion & biofilm formation on surfaces

- Cells exceed the ~250 nm acoustic penetration depth — the ΔD signal dominates, reporting contact points not total mass.
- The ΔD–Δf plot resolves stages: initial adhesion → attachment points → spreading → ECM production.
- Cytoskeleton drugs, apoptosis and cell lysis give distinct ΔD–Δf signatures in real time.
- Bacterial adhesion / biofilm growth and antibacterial action are followed label-free — key for implant surfaces.

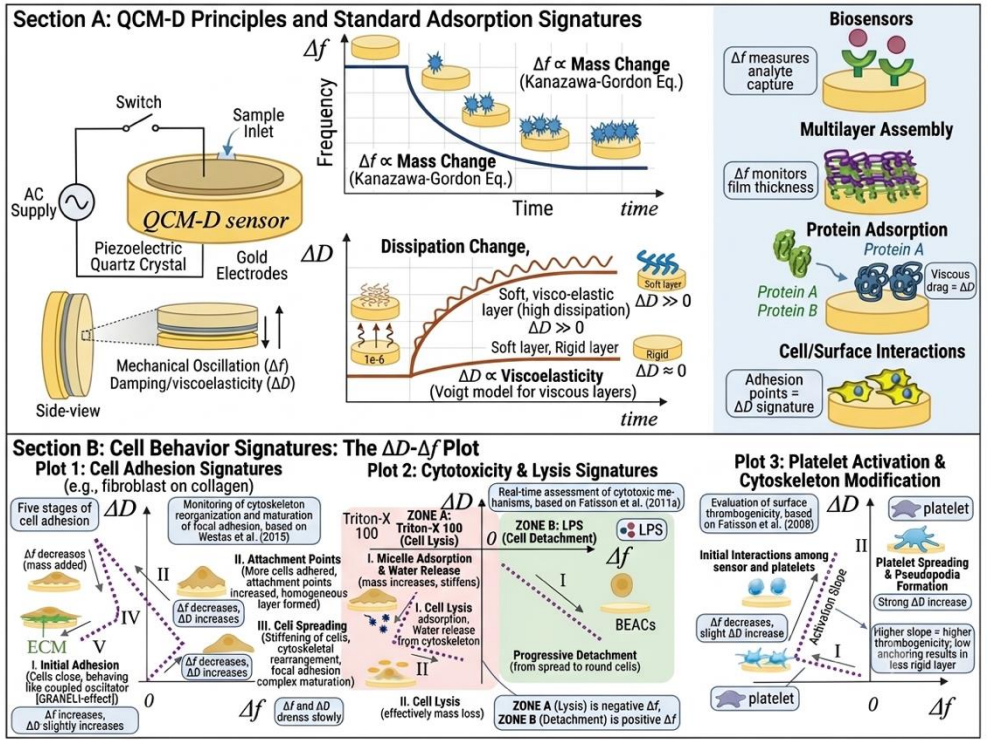

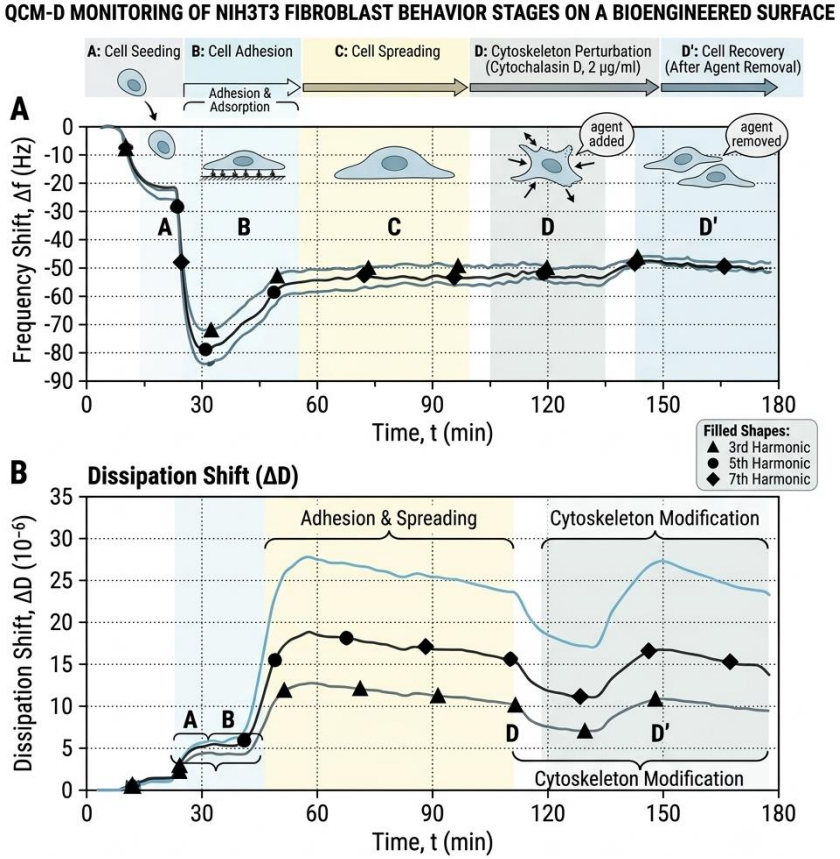

On electrified, bioengineered surfaces QCM-D predicts in-vivo cell behavior no optical assay captures.

SYNTHESIS

What each study contributes

Application	Signal read-out	Source figure
SAM biosensing platforms	Δf / ΔD per build step	**Valenti Fig 1 & 3 · Fogel Fig 1**
Protein adsorption + conformation	Δf mass, ΔD viscoelasticity	**Dixon Fig 2**
Antibody & DNA recognition	Coupled Δf + ΔD on binding	**Suthar Fig 3 · Dixon Fig 2**
Enzyme electrodes / biofuel cells	Current + mass + rheology	**Fogel Fig 2 & 5**
Cells & biofilms	ΔD–Δf stage signatures	**Tonda-Turo Fig 1 & 2**
EQCM-D coupling	Acoustic + EIS impedance	**Suthar Fig 1 & 6**

Across all five topics the pairing of Δf and ΔD — extended by electrochemistry — is what turns a mass balance into a biointerface tool.

REFERENCES

Source papers

1. **Dixon, M. C. (2008)** QCM-D: Enabling Real-Time Characterization of Biological Materials and Their Interactions. J. Biomol. Tech. 19, 151–158.

2. **Fogel, R. & Limson, J. L. (2011)** Probing fundamental film parameters of immobilized enzymes — Part II: Electroanalytical estimation of immobilized enzyme performance. Enzyme Microb. Technol. 49, 153–159.

3. **Valenti, L. E. et al. (2013)** Ni(II)-modified solid substrates as a platform to adsorb His-tag proteins. J. Mater. Chem. B 1, 4921–4931.

4. **Tonda-Turo, C. et al. (2018)** QCM-D with Dissipation Monitoring: A Powerful Method to Predict the in vivo Behavior of Bioengineered Surfaces. Front. Bioeng. Biotechnol. 6, 158.

5. **Suthar, J. et al. (2023)** Amplified EQCM-D detection of extracellular vesicles using 2D gold nanostructured arrays fabricated by block copolymer self-assembly. Nanoscale Horiz. 8, 460–472.

ELECTROCHEMICAL QUARTZ CRYSTAL MICROBALANCE

EQCM in Electrochemical Capacitors

Gravimetric insight into ion fluxes, solvation and charge-storage mechanisms in EDLCs, pseudocapacitors and conducting polymers

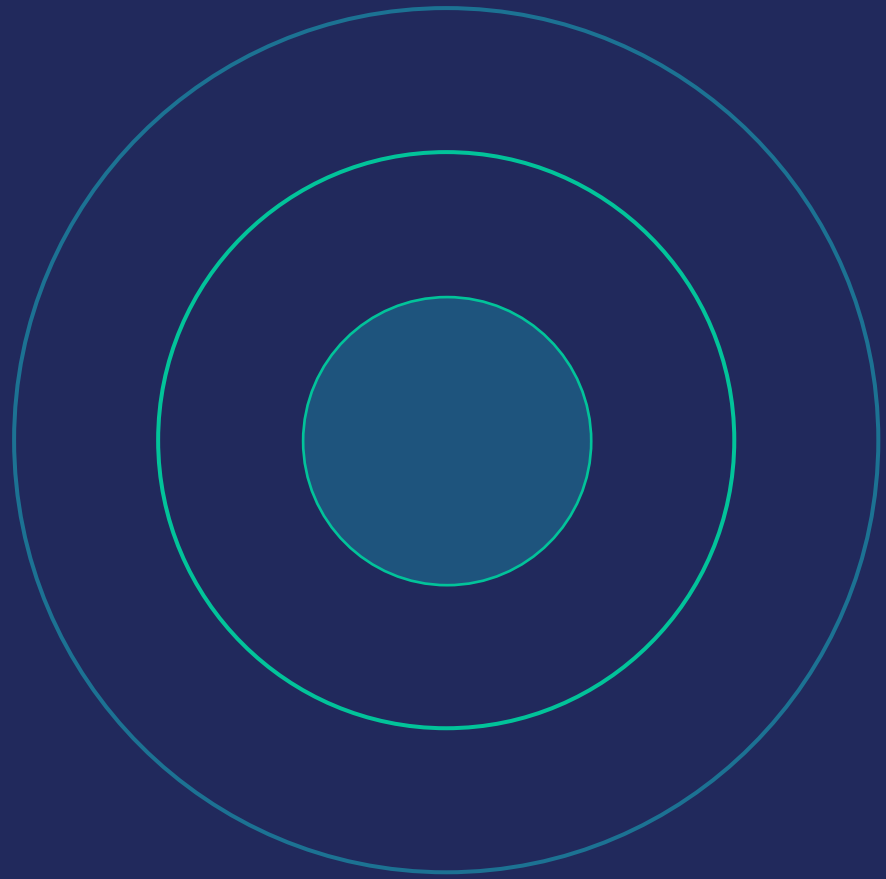

Supercapacitors module · ~20 min

ROADMAP

Outline

1. **EQCM fundamentals for capacitive storage**
   Sauerbrey equation, gravimetric CVs, PZC as the compass of ion fluxes
2. **EDL vs. pseudocapacitive contributions**
   How mass–charge signatures separate the two mechanisms
3. **Which ions carry the charge in carbon EDLCs?**
   Counter-ion adsorption, co-ion desorption, ion exchange & permselectivity
4. **Solvent and (de)solvation in confined pores**
   Solvation numbers, partial desolvation, pore-size effects
5. **Pseudocapacitive oxides & conducting polymers**
   MnO_2 / RuO_2, MXenes; PEDOT & PANI proton/anion fluxes (EQCM-D)
6. **Beyond Δf: ac-electrogravimetry**
   EIS + EQCM to deconvolute cation / anion / solvent dynamics

FUNDAMENTALS

The PZC is the compass of ion fluxes

- **EQCM cell: carbon-coated quartz sensor = WE, in a 3-electrode cell (CE + RE)**
- Potential of zero charge (PZC) separates two charge-carrier regimes:
  - ϕ > PZC → anion adsorption compensates positive charge
  - ϕ < PZC → cation adsorption compensates negative charge
  - Near the PZC → mixed ion exchange (counter-ion in / co-ion out)
- Landmark: activated carbon in 0.5 M CsCl — mass change follows polarization; higher overpotential vs. PZC = more permselective electrode
- PZC is set by carbon–electrolyte interactions: local structure, doping, surface groups → it can be engineered

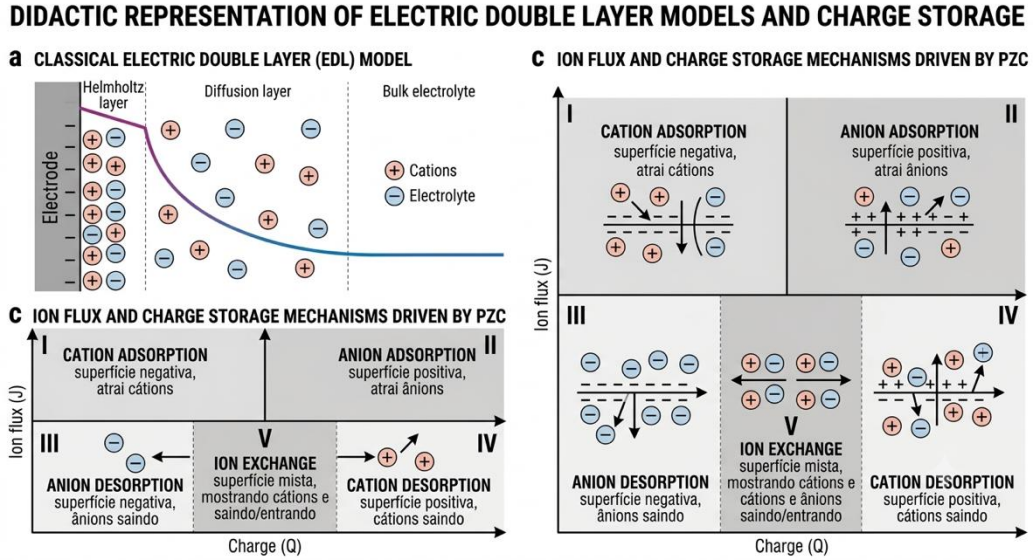

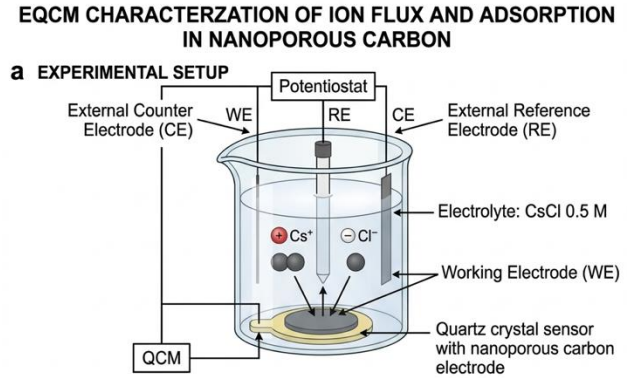

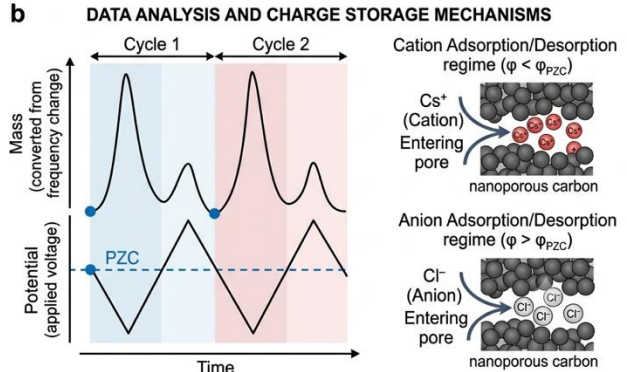

MECHANISM DISCRIMINATION

Distinguishing EDL from pseudocapacitive contributions

EDL (electrostatic)

- Rectangular CV; mass change tracks ion adsorption/desorption only
- Δm vs. ΔQ linear, slope ≈ molar mass of the adsorbing ion (Faraday's law)
- Raman bands of graphene-like carbons remain unchanged during charging

Functionalized carbons blur the line: oxidized YP50 (o-YP50) shows +73% capacitance at pH 1 vs. pristine carbon — redox activity of O-groups + surface-charge effects superimposed on the EDL.

Pseudocapacitive (faradaic)

- Redox bumps in CV; gravimetric CV (−dΔm/dt vs. E) shows peaks aligned with current peaks → ion (de)intercalation
- MnO2 (NMO): surface pseudocapacitance at low charge density → intercalation pseudocapacitance at high charge density (EQCM + in situ Raman)
- Charge depends on proton availability / surface redox groups, not only on ion adsorption

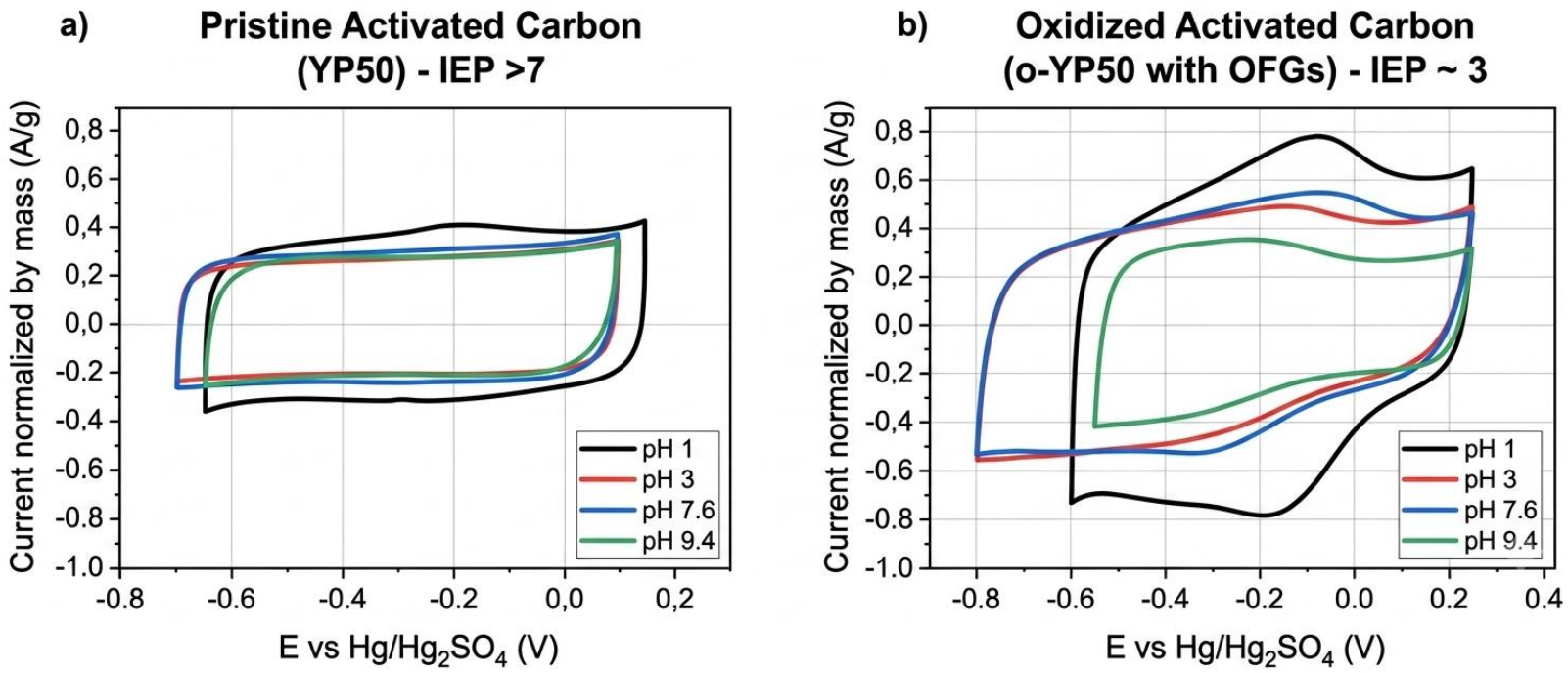

CARBON EDLCS

Which ions carry the charge? The slope test

- **Compare experimental mass–charge slope (ke) with the theoretical Faraday slope (kt) for bare counter-ion adsorption:**
  - ke < kt → ion exchange (counter-ion in + co-ion out)
  - ke = kt → pure (bare) counter-ion adsorption
  - ke > kt → adsorption of partially/fully solvated counter-ions
- YP-17 in CsCl: ion exchange at low charge density → counter-ion adsorption as charge density grows; water enters pores at high polarization (electrode expansion)
- Ion sieving: $TMA^+ < TEA^+ < TBA^+ < TOA^+$ — bulky cations shift the ion-exchange region and lose access to micropores
  - Concentration matters: 0.025 → 0.1 M CsCl widens the ion-exchange voltage window

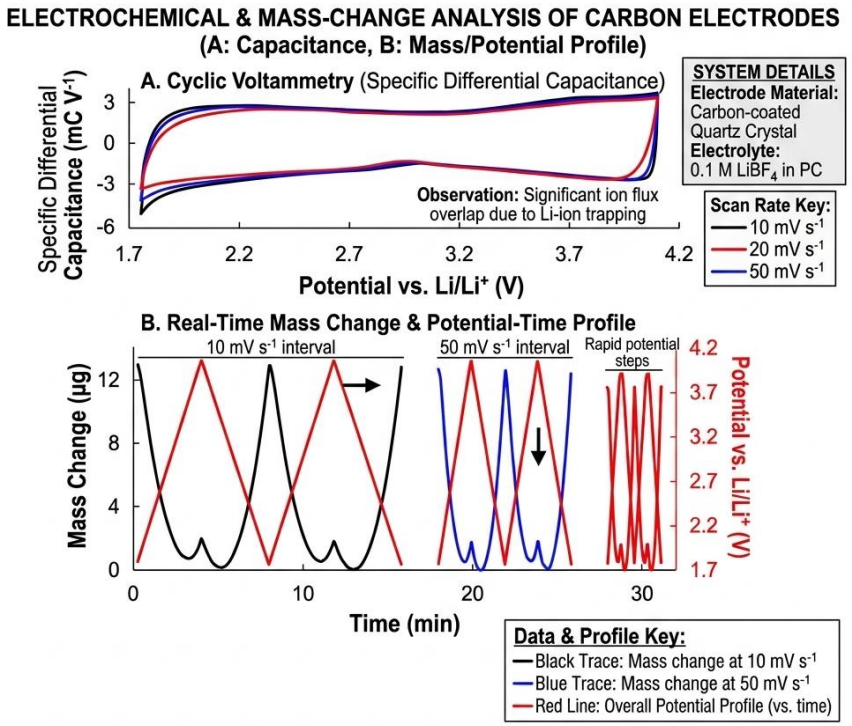

Figure. Cyclic Voltammograms (presented as differential capacitance) (**A**) and associated mass changes (**B**) for carbon-coated quartz crystal electrodes in 0.1 M $LiBF_4$ / PC. The colors indicate scan rates: **black** (10 mV s^{-1}), **red** (20 mV s^{-1}), and **blue** (50 mV s^{-1}). Mass data in **B** is shown for the 10 and 50 mV s^{-1} rates, while the overall potential profile (red line) tracks potential timing for all rates and rapid potential steps. Note the considerable overlap of cation flux-out and anion flux-in due to Li-ion trapping at high negative charge densities.

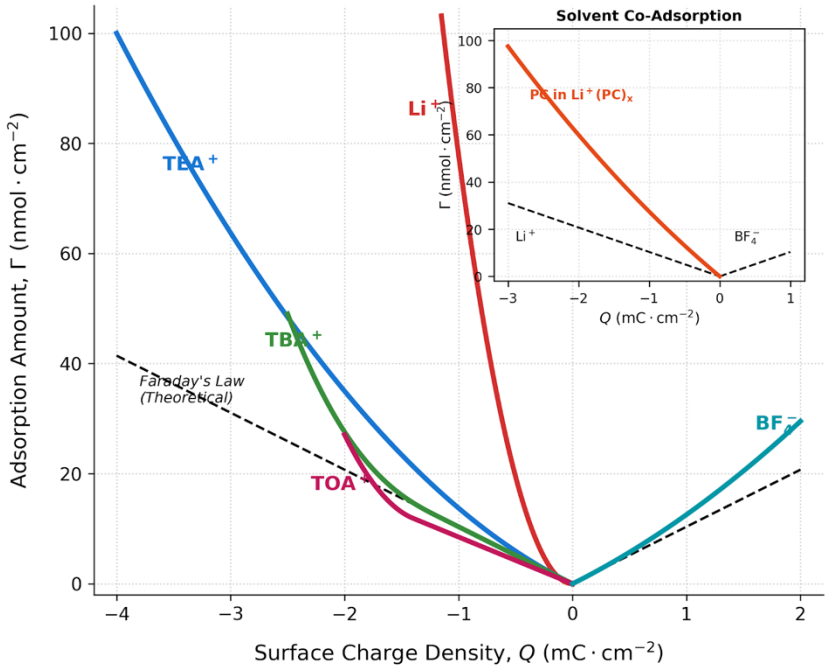

CARBON EDLCS — CASE STUDY

Surface chemistry & pH select the charge carrier

- **YP50 vs. oxidized o-YP50 in 0.5 M K2SO4/H2SO4, pH 1 → 9.4 (EQCM + TPD-MS)**
- Anion-based mechanism at low pH → growing cationic contribution as pH increases
  - The crossover is set by the isoelectric point (IEP): IEP(o-YP50) ≈ 3; IEP(YP50) ≈ 9
  - Deprotonated –COOH groups charge the surface negatively → K^+ dominates compensation at basic pH
  - $H3O^+$ dominates at pH 1–3 (high proton concentration); perm-selective failure lowers measured slopes
- dm/dt vs. E 'butterfly' plots reveal the crossover point (≈ PZC), shifting anodically with pH
- **Design rule: tune surface groups (IEP/PZC) + electrolyte pH to choose the working ion**

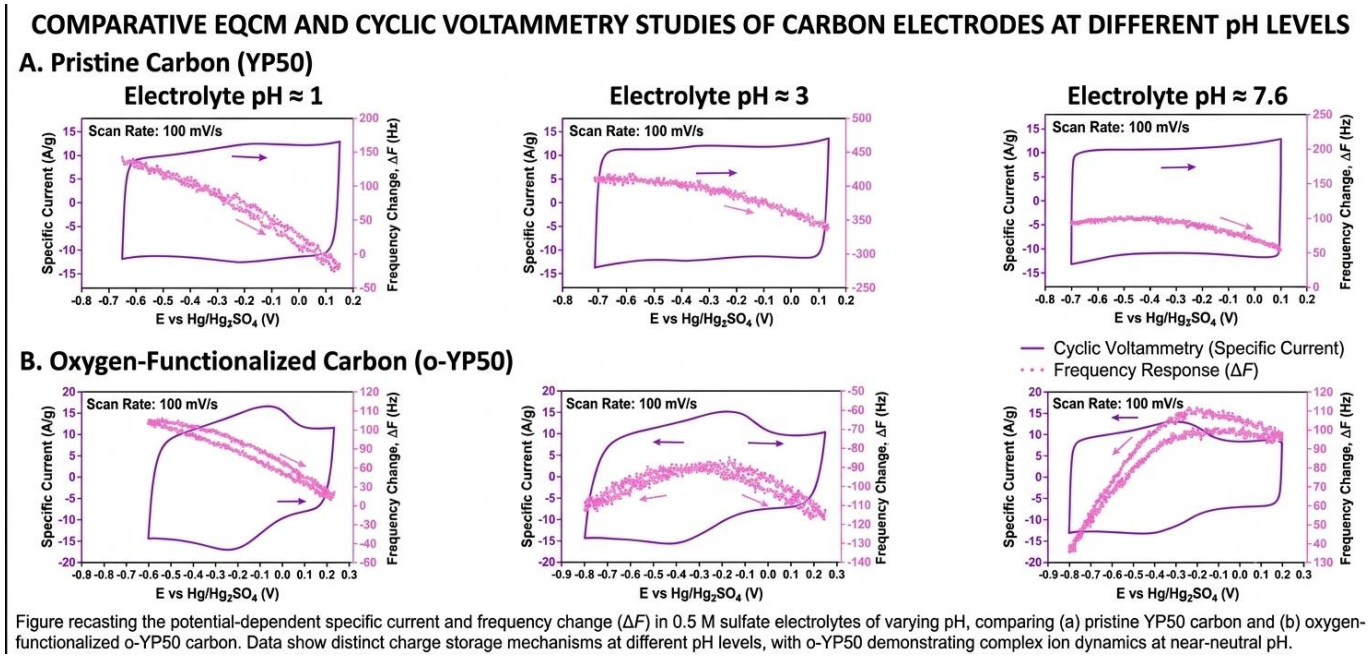

Figure recasting the potential-dependent specific current and frequency change (Δ*F*) in 0.5 M sulfate electrolytes of varying pH, comparing (a) pristine YP50 carbon and (b) oxygen-functionalized o-YP50 carbon. Data show distinct charge storage mechanisms at different pH levels, with o-YP50 demonstrating complex ion dynamics at near-neutral pH.

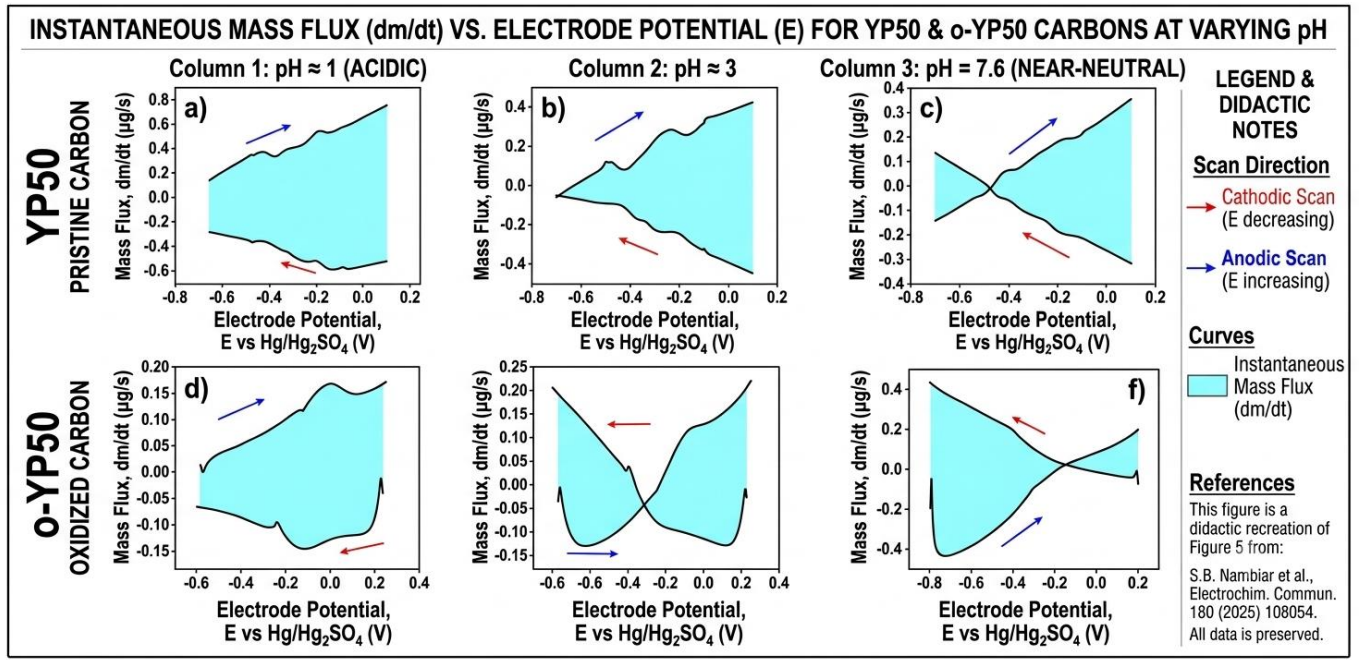

PSEUDOCAPACITANCE

Conducting polymers: PEDOT & PANI-type doping fluxes

- **p-type doping (PEDOT, PANI): oxidation creates holes compensated by anion uptake (or cation expulsion); reduction reverses the flux**
- PEDOT:PSS in 0.1 M NaCl (EQCM-D + CV):
  - De-doping at negative V = Na^+ uptake toward PSS^- sites; mass ↑ as holes are extracted
  - Ion-to-electron coupling efficiency ≈ 1 for thin films (1 Na^+ + ~2 H2O per hole); drops to ~0.2 thick films — water co-transport grows
- Ambipolar blends: EQCM assigns Cl^- injecti to p(g2T-TT) (p-doping) and K^+ injection to PrC60MA (n-doping) in the same film
- Caveats EQCM-D handles: swelling/viscoelasticity (Kelvin–Voigt fits), irreversible ion trapping, ORR side currents

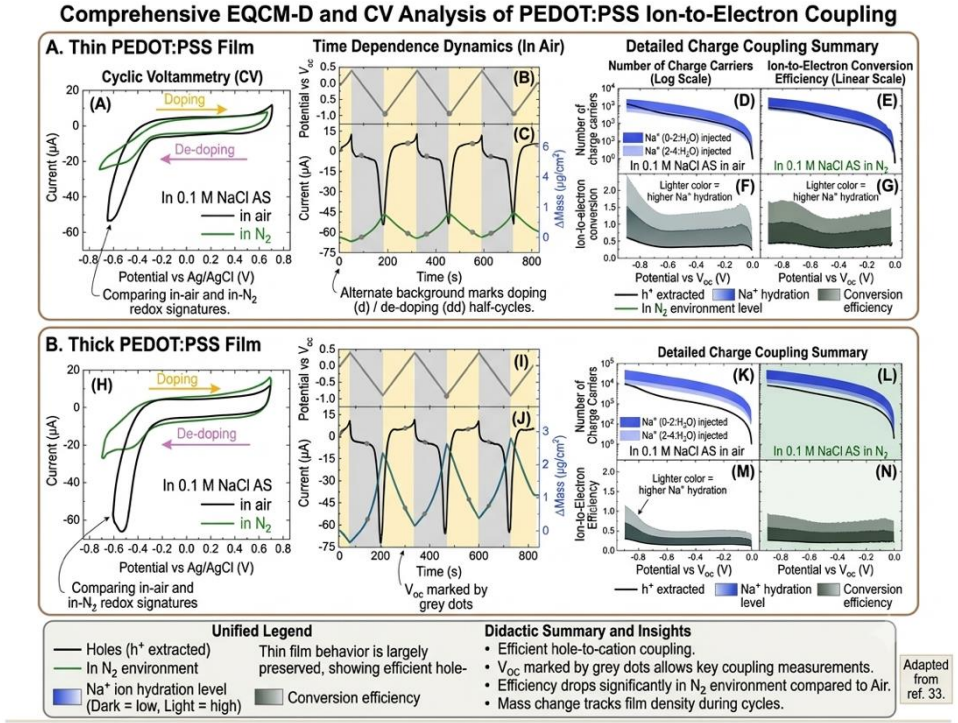

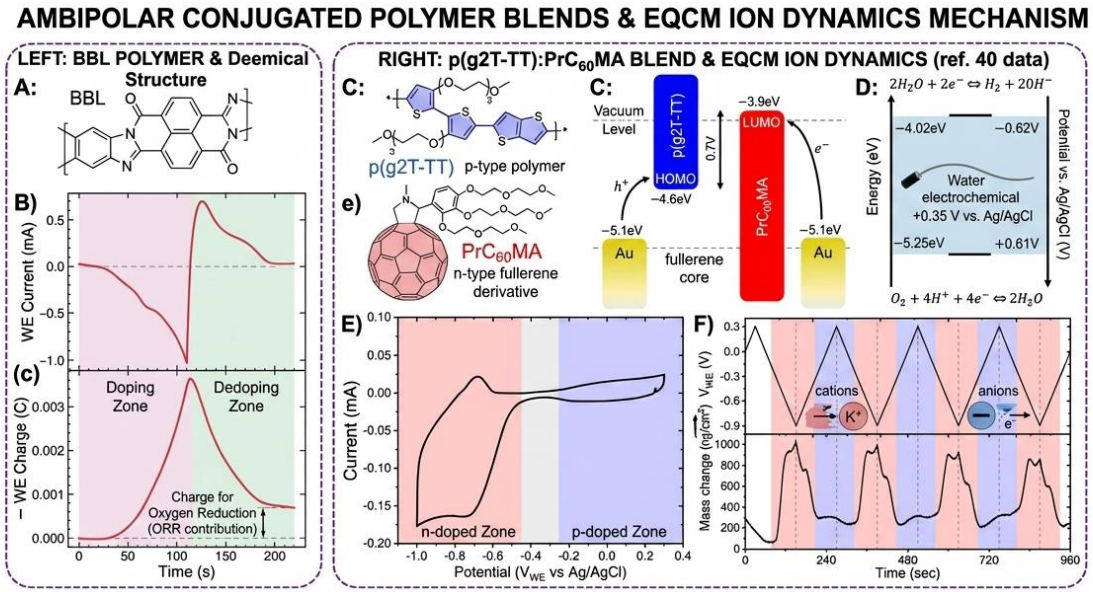

EQCM-D: when the film is soft

- **Dissipation factor D = E_dissipated / 2πE_stored — tracks viscoelasticity alongside mass**
- Sauerbrey fails for hydrated/swollen films → viscoelastic models (Kelvin–Voigt, Maxwell, extended Voigt) fit multi-overtone Δf, ΔD data
  - Overtones probe different depths → depth-resolved kinetics (fast ion migration vs. slow matrix reorganisation in PEDOT:PSS)
- For rigid porous carbons: verify motional resistance is negligible before applying Sauerbrey (done in the pH study of YP50)
- Applications: swelling, water uptake, adhesion/delamination, degradation & ORR contributions

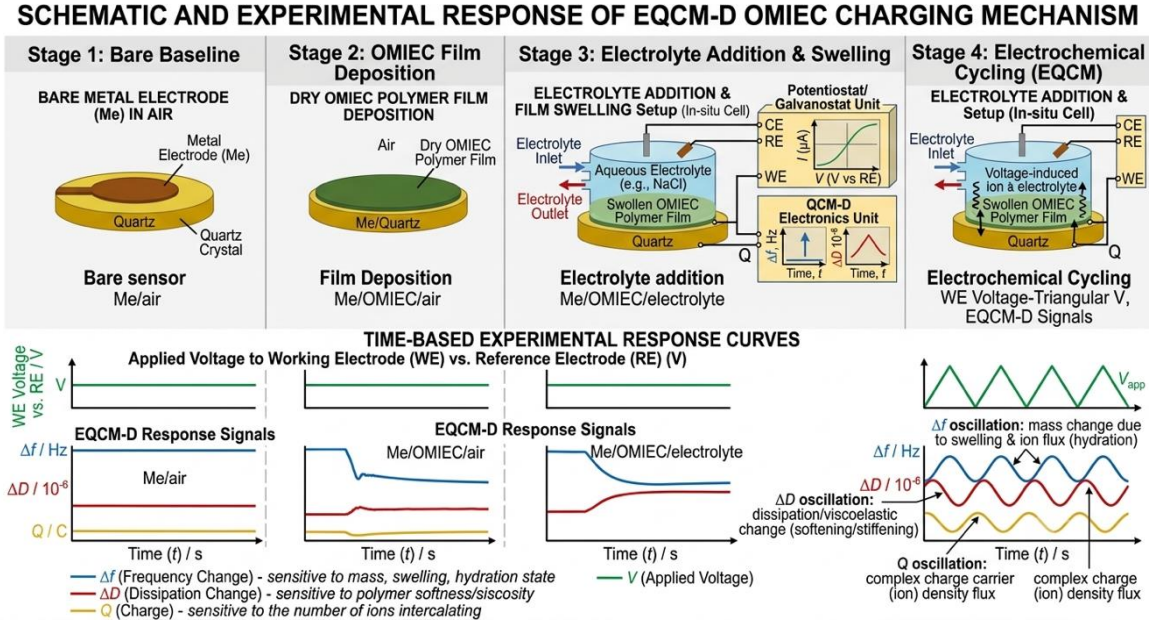

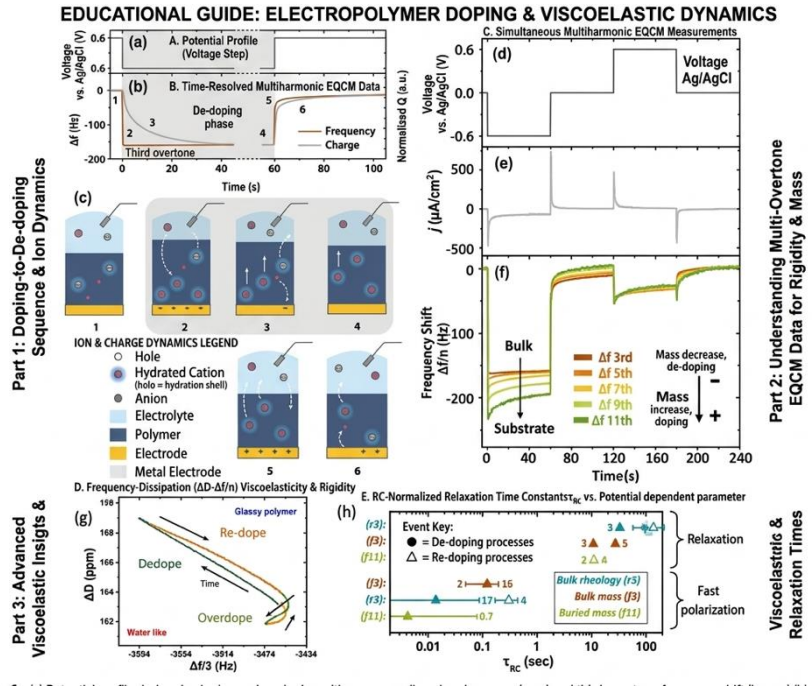

TAKE-HOME MESSAGES

What EQCM tells us about capacitors

1. **Mechanism ID —** Δm–ΔQ slopes + gravimetric CVs separate EDL adsorption from redox-coupled (pseudocapacitive) ion fluxes.
2. **Ion selection —** PZC/IEP vs. applied potential (and pH, doping, surface groups) decides whether cations or anions compensate the charge.
3. **Solvent counts —** Solvation numbers from EQCM prove partial desolvation under confinement — a root of anomalous capacitance in sub-nm pores.
4. **Soft electrodes —** For MnO2, MXenes, PEDOT/PANI: EQCM(-D) resolves proton/cation/anion fluxes, coupling efficiency, swelling & degradation.
5. **Next step —** ac-electrogravimetry (EIS + QCM) deconvolutes cation, anion and solvent dynamics — toward fully quantitative pictures.

SOURCES

Key references

Niu, L. et al. Understanding the charging of supercapacitors by EQCM. Ind. Chem. Mater. 2023, 1, 175–187. *Figs. 2–6, Table 1, Eqs. (1),(5),(6)*

Levi, M. D. et al. EQCM studies of ions and solvents insertion into highly porous activated carbons. J. Am. Chem. Soc. 2010, 132, 13220–13222. *Figs. 1–3 (solvation number of $Li^+ \approx 3$)*

Nambiar, S. B. et al. Probing the role of isoelectric point in charge storage of functionalized carbon by EQCM. Electrochem. Commun. 2025, 180, 108 054. *Figs. 2–5 (pH / IEP case study)*

Ge, K. et al. Advanced characterization of confined electrochemical interfaces in electrochemical capacitors. Nat. Nanotechnol. 2025, 20, 196–208. *Figs. 1–3 (PZC, confinement, EQCM + Raman)*

Mukhin, N. et al. Electrochemical QCM-D for insights into OMIECs and OECTs. Mater. Chem. Front. 2026, 10, 694–740. *Figs. 3, 6, 7, 9; Table 3 (EQCM-D, PEDOT)*

IN SITU ELECTROGRAVIMETRY

EQCM in Batteries

Probing mass, ion fluxes, interphases and degradation of battery electrodes in real time

Based on: Wu et al. (ACS AMI 2015) · Levi et al. (Electrochem. Commun. 2016; Electrochim. Acta 2017) · Shpigel et al. (Acc. Chem. Res. 2018) · Park et al. (Hydrometallurgy 2026)

AGENDA · 25 MIN

Outline

1. **Probing intercalation & conversion electrodes**
   Li-ion, Na-ion / K-ion (alkali cations), Li–S conversion chemistry

2. **Quantifying ion & solvent (co-)insertion**
   Mass-per-charge analysis (Δm/σ), trapped vs. moveable electrolyte

3. **SEI formation & electrolyte decomposition**
   Viscoelastic probing of surface films, electrolyte screening

4. **Cycling stability & degradation markers**
   Irreversible frequency / resistance offsets, roughening, cracking

5. **Case study + outlook**
   SEI on a model anode (LTO); extension to Si anodes and recycling

Li-ion hosts: weighing Li^+ extraction in $LiFePO_4$

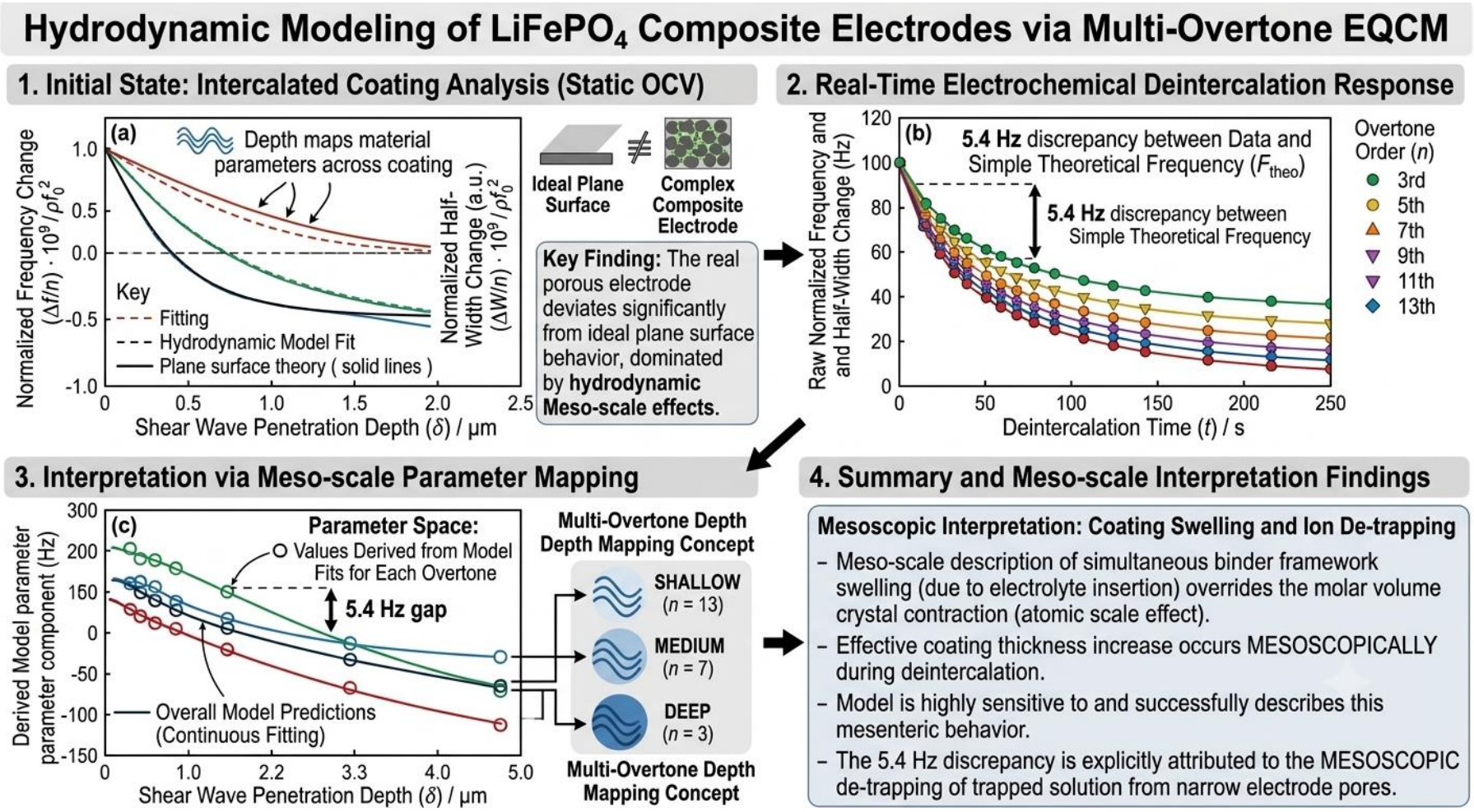

- Composite $LiFePO_4$ (PVdF binder) charged in aqueous Li_2SO_4 — rigid coating, clean model system
- Experimental Δf/n smaller than Faraday prediction (F_theo): ~5.4 Hz gap = electrolyte entering the porous electrode
- Effective thickness h increases ~1 % on deintercalation, while in-situ XRD shows ~6 % particle contraction → solution swells the electrode on the mesoscale
- Message: even a 'simple' intercalation host is never purely gravimetric — hydrodynamic correction is required

Alkali-cation insertion ($Li^+ \rightarrow Cs^+$): MXene as a 2D host

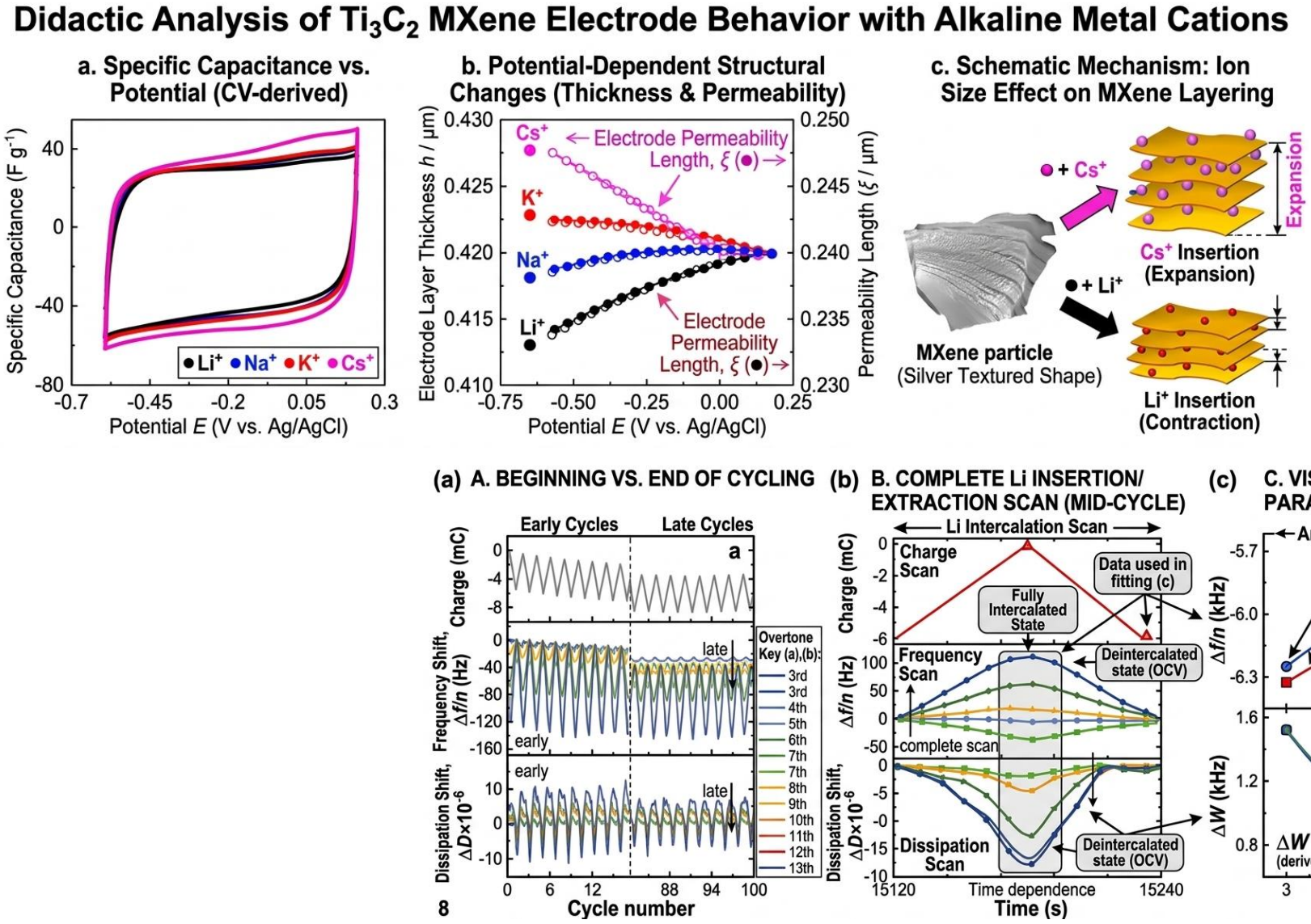

- Same methodology transfers directly to Na-ion / K-ion chemistry: cation identity read out through deformation sign and magnitude
- CV curves for Li^+…Cs^+ look alike — EQCM-D distinguishes them via opposite Δh, Δξ trends
- Water and Li^+ (de)insertion cause reversible softening / stiffening of the MXene host (H-bond network modulation)
- Mesoscopic, ion-specific structural information inaccessible to in-situ XRD

Li–S: weighing polysulfide formation on a S–C cathode

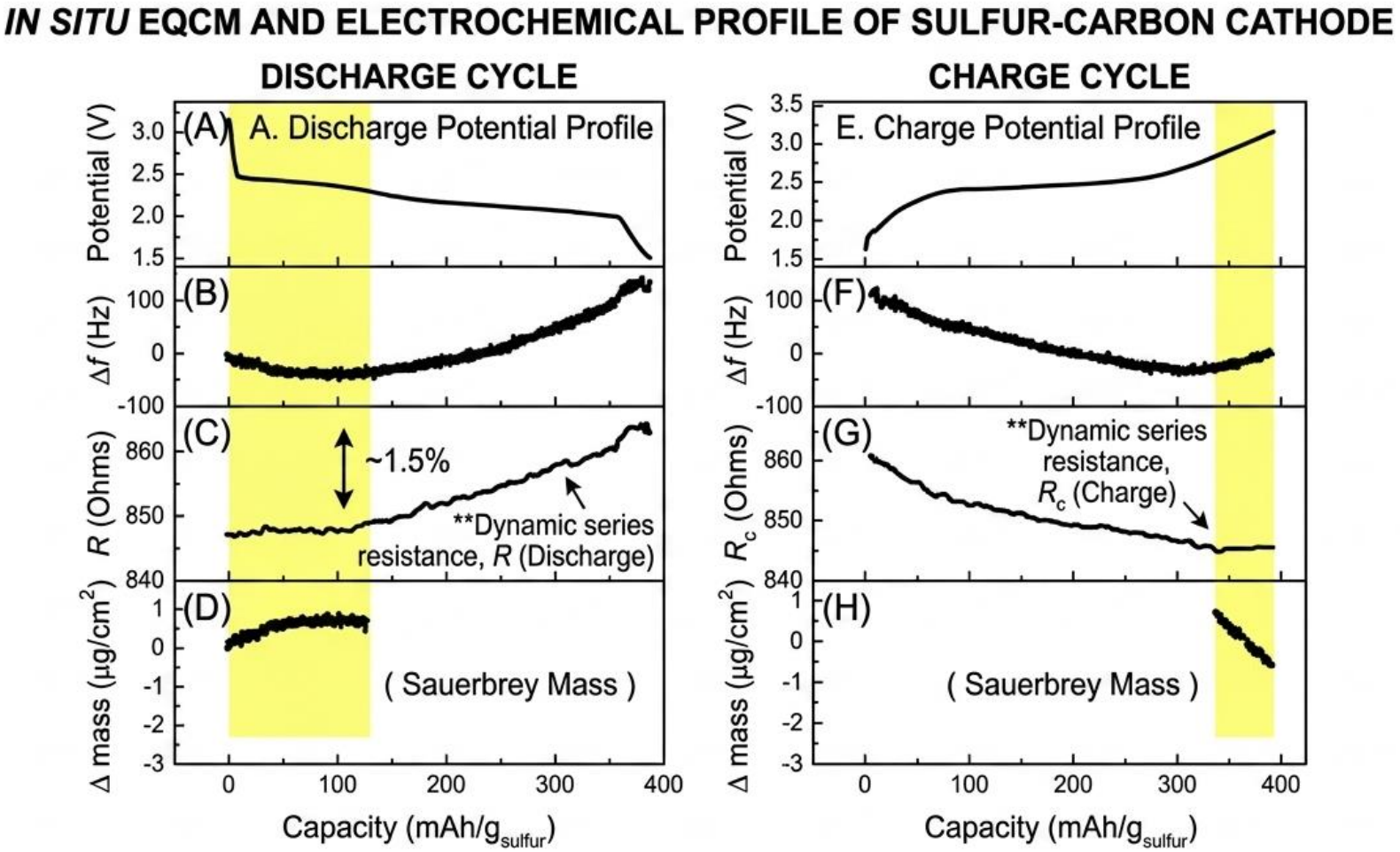

- First discharge plateau (~2.4 V): mass gain ≈ 0.77 μg cm^{-2} from S_8 ring opening / lithiation to long-chain Li_2S_8, Li_2S_6
- Measured gain ~35 % below the charge-based prediction → ~35 % of active sulfur dissolves into the electrolyte
- Below 2.4 V: crystal resistance R_c rises — Sauerbrey no longer valid; the 'mass' signal becomes electromechanical
- Monitoring R_c (≈ dissipation) alongside Δf is essential for conversion chemistries with large volume/roughness changes

Quantifying (co-)insertion: the mass-per-charge ratio

$\Delta\Gamma = \Delta m / M_i = \sigma / (|z_i| \cdot F)$ → $\Delta m/\sigma$ vs. $M_i /(|z_i|F)$

Compare EQCM mass flux with Faradaic charge: equality = bare-ion insertion; excess = solvent co-insertion; deficit = co-ion / expulsion effects.

- Perm-selectivity in porous carbons: near pzc both counter- and co-ions move (perm-selectivity failure); at higher charge, counter-ions dominate
- Solvation numbers of confined ions and neutral-solvent fluxes extracted from the Δm–σ mismatch
- Caveat: EQCM weighs the balance only — solvated ion vs. ion + separate solvent needs complementary techniques (e.g., in-situ NMR)

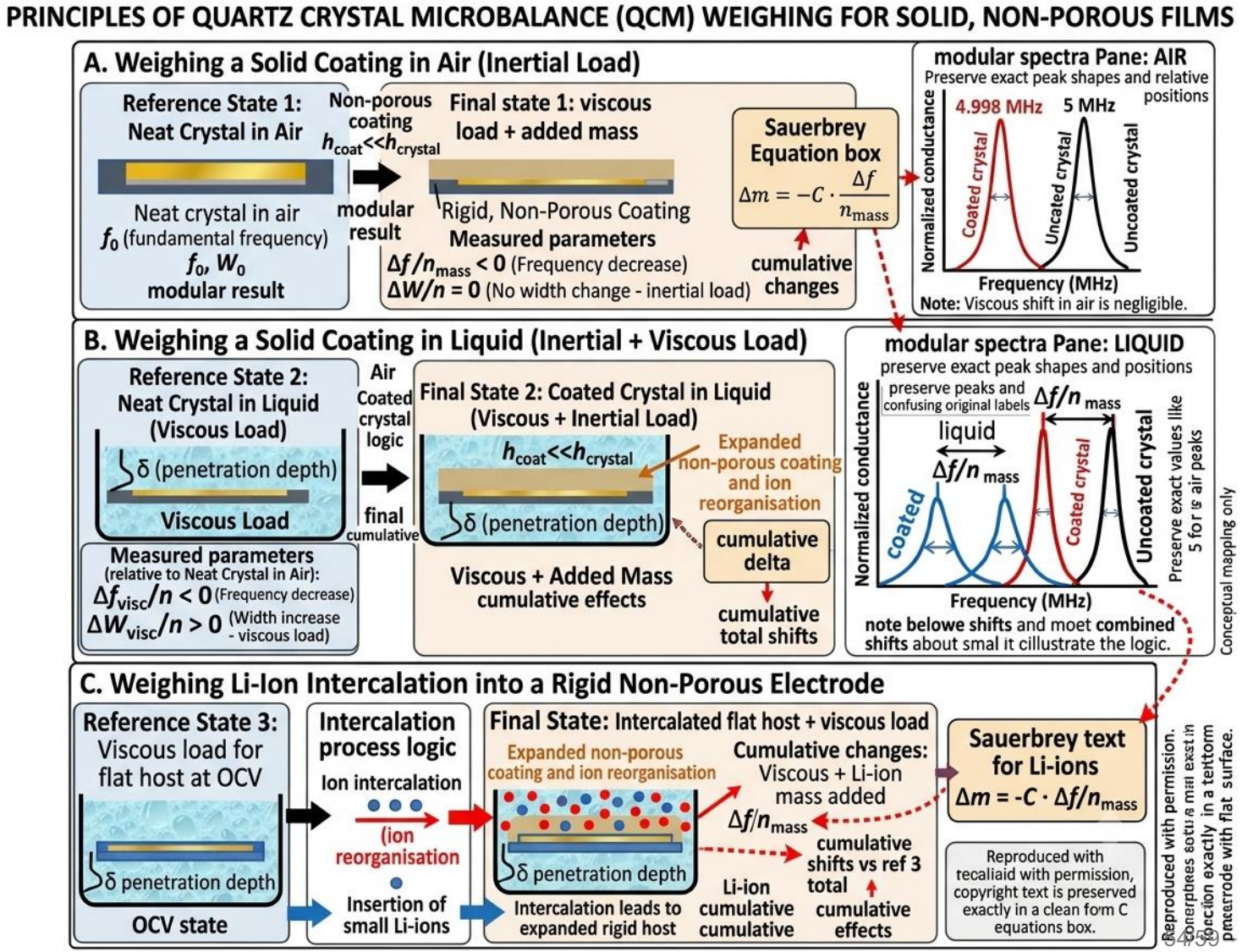

Quantifying (co-)insertion: the mass-per-charge ratio

$\Delta\Gamma = \Delta m / M_i = \sigma / (|z_i| \cdot F)$ → $\Delta m/\sigma$ vs. $M_i /(|z_i|F)$

Compare EQCM mass flux with Faradaic charge: equality = bare-ion insertion; excess = solvent co-insertion; deficit = co-ion / expulsion effects.

- Perm-selectivity in porous carbons: near pzc both counter- and co-ions move (perm-selectivity failure); at higher charge, counter-ions dominate
- Solvation numbers of confined ions and neutral-solvent fluxes extracted from the Δm–σ mismatch
- Caveat: EQCM weighs the balance only — solvated ion vs. ion + separate solvent needs complementary techniques (e.g., in-situ NMR)

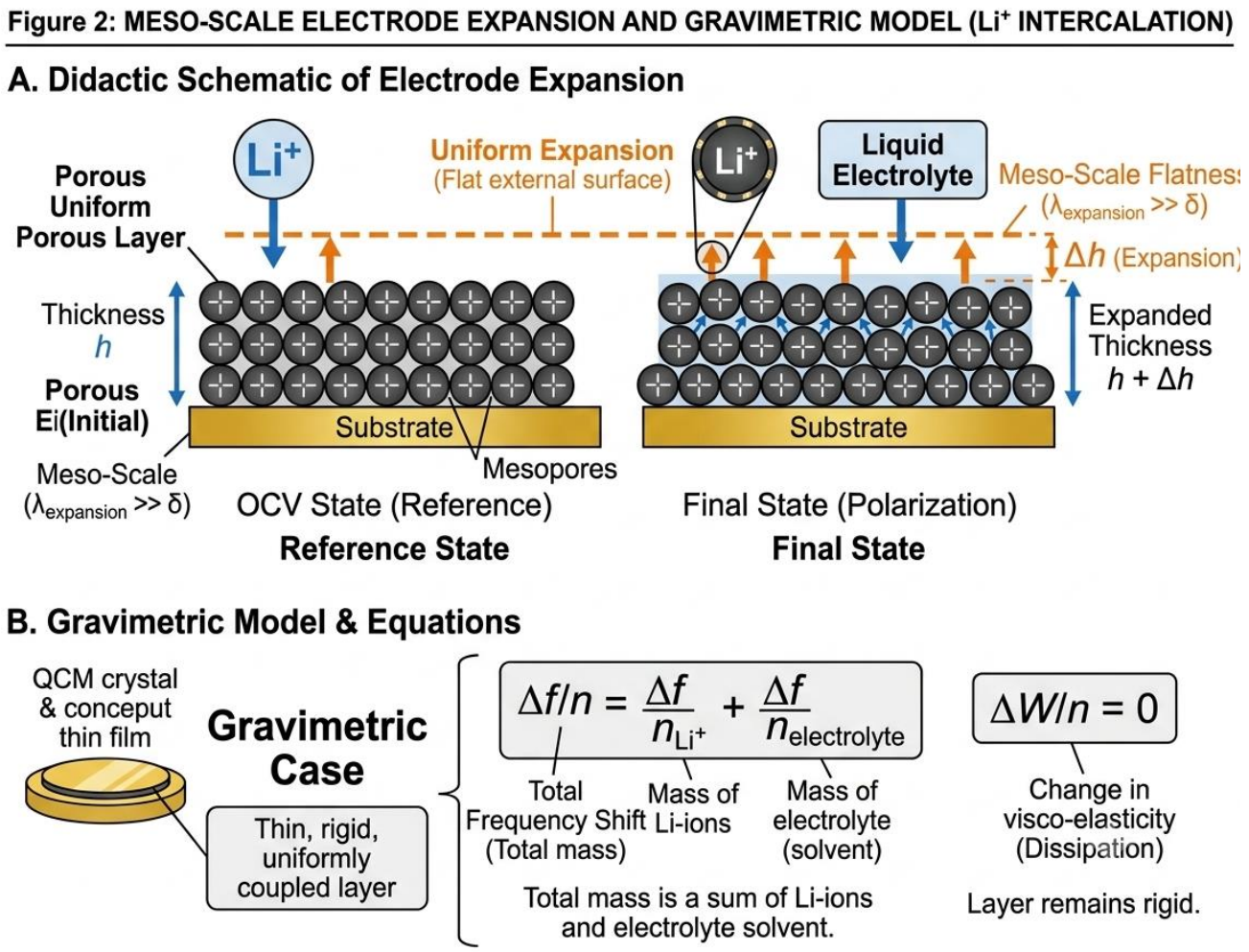

2 · ION & SOLVENT FLUXES

Trapped vs. moveable electrolyte: probing with δ(n)

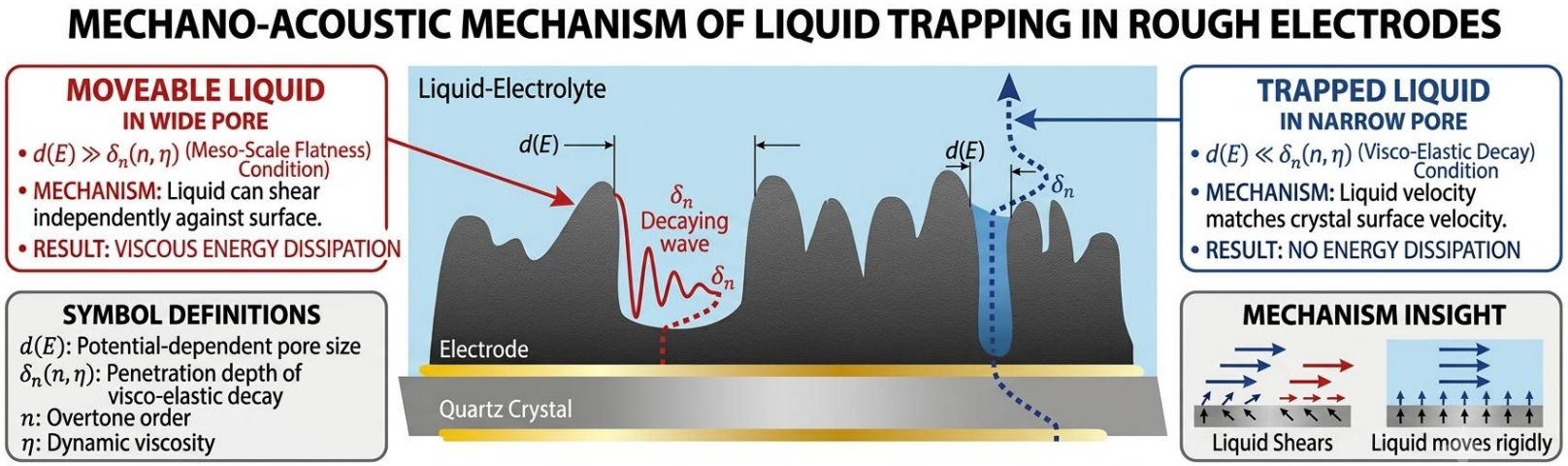

Fig. 9. Detailed schematic illustrating the mechano-acoustic mechanism of visco-al-elastic decay of transverse oscillation waves (δ_n) at a rough/porous electrode in contact with an electrolyte liquid. The color-coded callouts explain the energy dissipation based on pore size relative to wave decay depth ($d(E)$ vs. δ_n), explicitly defining terms and showing the callout conditionsoot conditions. The dotted lines show the wave decay for the two different cases.

- Varying overtone order sweeps δ from ~240 to ~68 nm → instantaneous test of whether pore liquid moves with the electrode or dissipates
- Trapped liquid adds Sauerbrey mass; moveable liquid adds ΔW/n — the two are separable by multiharmonic fitting
- Potential-dependent pore width d(E): intercalation-induced squeezing / uptake of solution followed in real time
- Δm/σ + hydrodynamic terms together give a full ion + solvent budget per cycle

SEI formation & electrolyte decomposition, watched live

- SEI = reduction products of the electrolyte; a good film is thin, dense, mechanically robust, Li^+-conducting
- EQCM-D separates gravimetric intercalation from film growth: mass gain + evolving viscoelasticity (G′, G″, thickness) of the surface layer
- Onset potentials of decomposition read directly from CV + Δf: SEI 'starts here' at different E for LiTFSI vs. $LiPF_6$
- Dissipation reports film softness — early EQCM-D showed SEI rigidity decreasing with time (Yang et al., cited in Wu 2015)
- LTO chosen as a 'zero-strain' host → all mechanical signal comes from the surface film, not the electrode bulk
- Electrolyte screening (LiTFSI vs. $LiPF_6$ vs. $LiPF_6$ + 2 % VC): SEI quality ranked after a few fast cycles (~15–30 min)
- Same ranking needs ~100 slow cycles (200 h) in coin cells — EQCM-D as an accelerated diagnostic
- Best capacity retention correlates with the stiffest, thinnest SEI (LiTFSI system)
- Same protocol extends to graphite / Si and Sn anodes (Si: high-volume-change frontier; Sn SEI pioneered at Argonne)

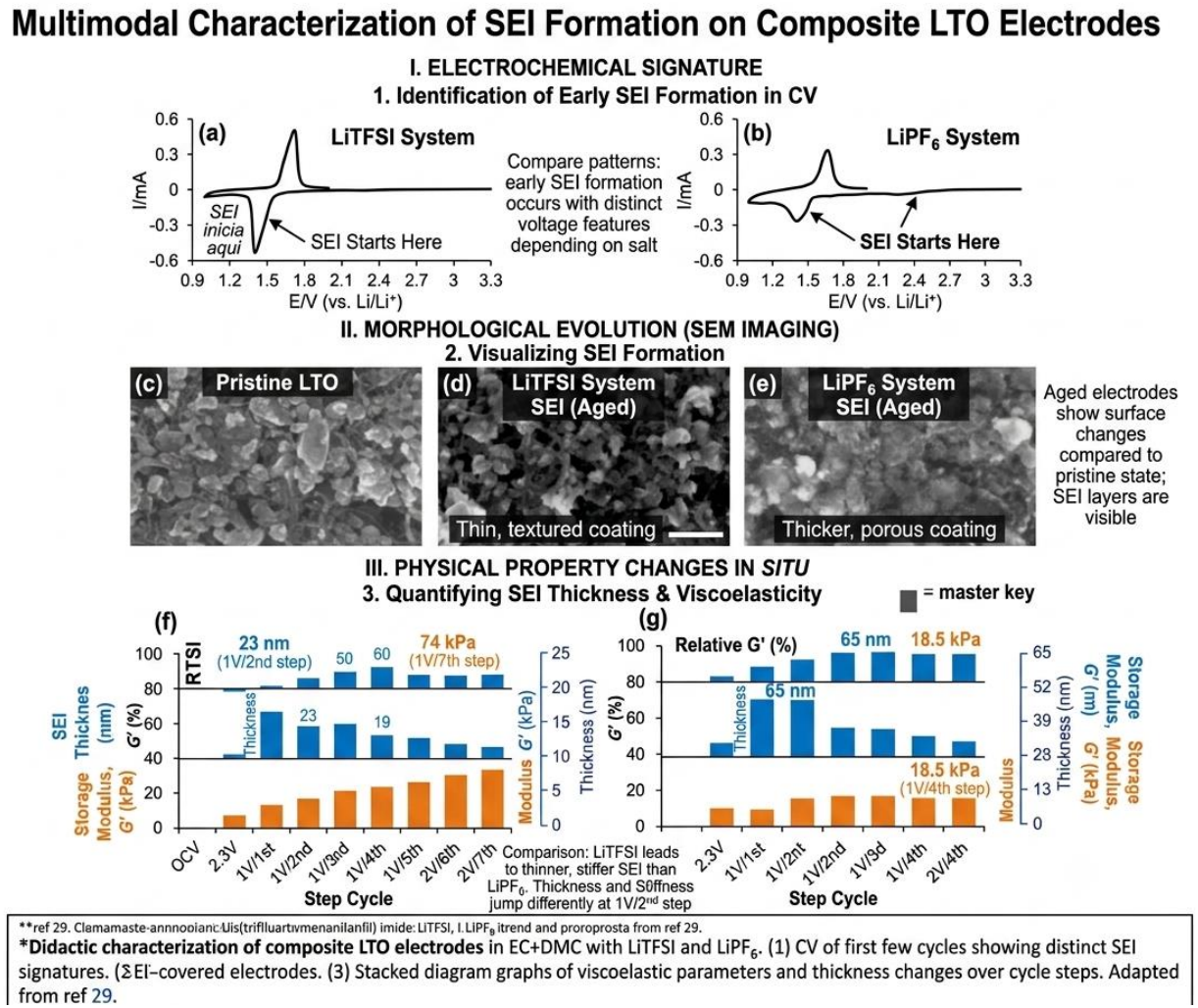

**ref 29. Clamamaste-annnoojanc:Lis(trifluartivmenanilanfil) imide: LiTFSI, I. $LiPF_6$ itrend and proroprosta from ref 29.
***Didactic characterization of composite LTO electrodes** in EC+DMC with LiTFSI and $LiPF_6$. (1) CV of first few cycles showing distinct SEI signatures. (ΣEI-covered electrodes. (3) Stacked diagram graphs of viscoelastic parameters and thickness changes over cycle steps. Adapted from ref 29.

Beyond cycling: EQCM for battery recycling ($LiCoO_2$ leaching)

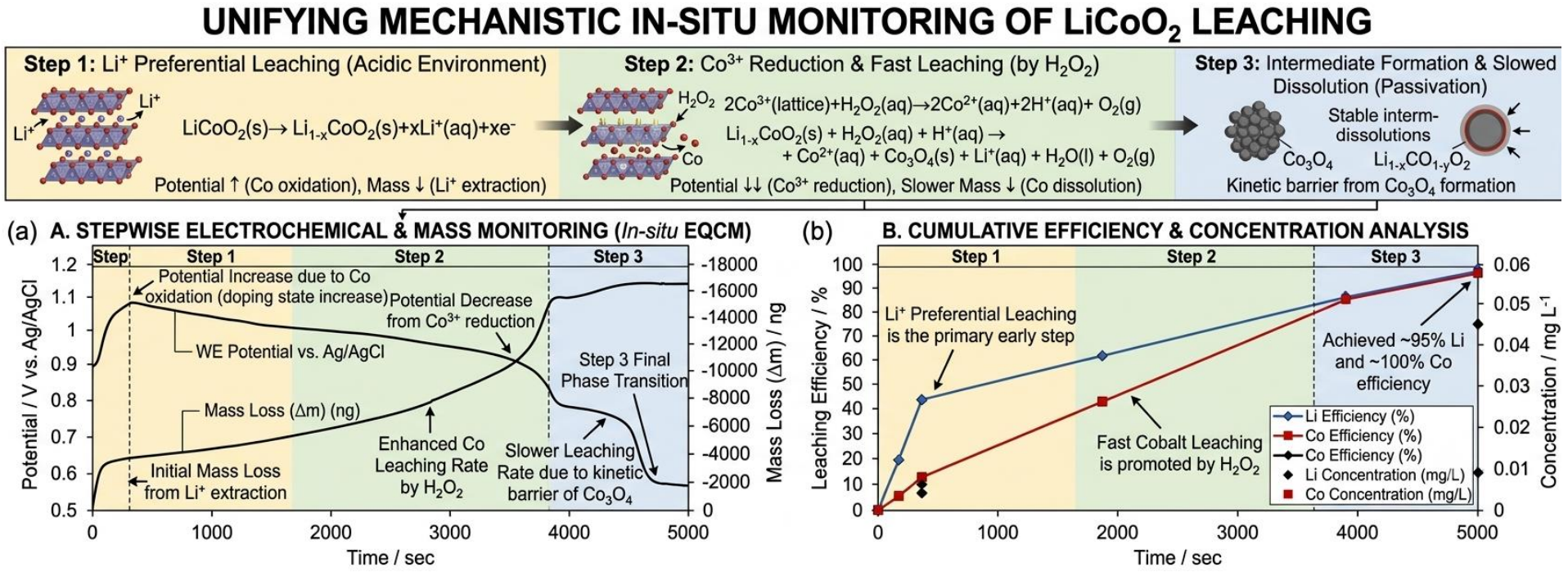

- First in-situ EQCM study of cathode leaching: OCP + mass loss resolve a stepwise mechanism in real time
- Step 1: preferential Li^+ extraction (43 % Li vs. 12 % Co) with rising potential — delithiation of the lattice
- Step 2: H_2O_2 reduces $Co^{3+} \rightarrow Co^{2+}$, accelerating dissolution but converting part of the film to Co_3O_4
- Step 3: Co_3O_4 acts as a kinetic barrier → slow residual leaching; suppressing it is key to complete Co recovery
- Same crystal, opposite problem: EQCM guides selective metal recovery, not just electrode operation

TAKE-HOME MESSAGES

Conclusions

- EQCM weighs ion (de)insertion at ng cm^{-2} resolution — but only where $\Delta W/n \approx 0$; always check dissipation / R_c first
- Multiharmonic EQCM-D adds mesoscopic structure: porosity, thickness, roughness and their potential dependence (in-situ hydrodynamic spectroscopy)
- Mass-per-charge analysis quantifies solvent co-insertion and perm-selectivity; trapped vs. moveable electrolyte is separable via δ(n)
- SEI mechanics (G', thickness) enable electrolyte screening in minutes instead of weeks
- Irreversible Δf / ΔR_c offsets are early, quantitative degradation markers — validated by SEM
- Emerging uses: alloy anodes (Si) with MOSS coupling, ac-electrogravimetry, and hydrometallurgical recycling

Sources: Wu et al., ACS Appl. Mater. Interfaces 2015, 7, 20820 · Levi et al., Electrochem. Commun. 2016, 67, 16 · Levi et al., Electrochim. Acta 2017, 232, 271 · Shpigel et al., Acc. Chem. Res. 2018, 51, 69 · Park et al., Hydrometallurgy 2026, 241, 106655